ISEIS

Journal of Environmental Informatics 40(2) 157-175 (2022)

Journal of Environmental Informatics

www.iseis.org/jei

EVI Indicated Spatial-Temporal Variations in Vegetation and Their Responses to Climatic and Anthropogenic Factors in the Chinese Mainland Since 2000s

Z. Yuan[1 *], J. J. Xu[1], J. Chen[1], Y. Q. Wang[1], and J. Yin[2]

[1] *Changjiang River Scientific Research Institute, Changjiang Water Resources Commission of the Ministry of Water Resources of China, Wuhan 430010, China*

[2] *Faculty of Resources and Environmental Science, Hubei University, Wuhan 430062, China*

Received 29 Feburary 2020; revised 16 April 2020; accepted 13 March 2021; published online 13 August 2021

ABSTRACT. Terrestrial ecosystems of China play an important role in global carbon cycle. Identifying spatial-temporal variation of vegetation and their driving forces in China is necessary. This study used recent Enhanced Vegetation Index (EVI) data (2000 to 2019) to analyze interannual changes of vegetation activity in mainland China, and examined their responses to climatic (precipitation and temperature) and anthropogenic factors (human land-use management such as afforestation, cultivation and urbanization). The results showed an increasing trend in EVI over the 20-year period, which strikingly prominent in Loess Plateau. Besides, the greening rate of mainland China over 2009 ~ 2019 was weaker than that for 2000 to 2008. The wetter and warmer climatic condition in recent 20 years is conducive to vegetation growth in mainland China. In addition, human activities, such as implementation of ecological restoration programs, construction of irrigated areas and heavy fertilizer use promote the vegetation growth in forestland and cultivated land. While the browning in some vegetated land might relate to urbanization. Although climatic and anthropogenic factors both contributed to vegetation change, our results indicated that the anthropogenic factors were the key drivers. In more than half of the significant greening or browning region (51.2%), EVI change were dominant by human activities (explain more than 60% of the significant trend). However, climate change was a dominant driver of EVI change over only 9.9% of significant greening or browning region. The findings of this study provided details of EVI variations and their mechanics in mainland China, which can provide useful information for government organizations.

Keywords: vegetation variation, climate change, human activities, the Chinese Mainland

1. Introduction

Vegetation plays an important role in energy transfer, carbon cycle, water balance and climate regulation, acting as a key component of terrestrial ecosystem (Bégué et al., 2011). The satellite remote sensing provides an advanced way to monitor vegetation activity with continuous spatial-temporal products. Vegetation greening trend has been detected at regional and continental scales based on the satellite measurements, especially in China and India (Zhu et al., 2016; Zhao et al., 2018). However, vegetation browning trends were also found in some areas of Southern Hemisphere (Zhao and Running, 2010). In general, both climatic and anthropogenic environmental changes would affect vegetation characters, such as distribution and productivity, which might lead to vegetation greening and browning (Kuenzer et al., 2015; Zheng et al., 2019). Investigating the vegetation changes and their responses to environmental factors can improve stakeholders' ability of prediction, mitigation and adaption in changing environment (Sitch et al., 2008; Piao et al., 2014). The Normalized Difference Vegetation Index (NDVI) and Enhanced Vegetation Index (EVI) have been widely used for global and local monitoring of vegetation conditions (Setiawan et al., 2014; Peng et al., 2019; Ahmed and Singh, 2020; Vijith and Dodge-Wan, 2020). By minimizing canopy background variations and removing residual atmosphere contamination, EVI has the advantage in monitoring sensitive and high biomass conditions comparing with NDVI (Huete et al., 2002; Fraga et al., 2014).

The precipitation and temperature are important climatic factors for vegetation growth and have been selected for analyzing the effect of climate change on vegetation activity in regional or global scales (Daham et al., 2018; Muradyan, et al., 2019; Szabó, et al., 2019). Human land-use management also has a profound impact on growth and greening of vegetation (Zhu et al., 2016). Vegetation change and relationship with direct or indirect drivers are often revealed by linear regression and correlation analysis (Raynolds et al., 2008; Zhang et al., 2019). Generally speaking, the influences of environmental perturbations and changes are spatial heterogeneity and complexity. Previous studies proven that vegetation was limited to temperature in northern high-latitudes while limited to water in arid and semi-arid regions (Piao et al., 2009; Zhou et al., 2015; Zhao et al., 2018). For instance, large-scale greening in Africa were mainly caused by precipitation (Adole et al., 2018). The rising temperature in Tibetan Plateau enhances photosynthesis

* Corresponding author. Tel.: +86-137-1656-5927
E-mail address: yuanzhe_0116@126.com (Z. Yuan).

ISSN: 1726-2135 print/1684-8799 online
 doi:10.3808/jei.202100467

and lengthens the growing season, which has positive effects on vegetation growth in Tibetan Plateau (Xu et al., 2013). The urbanization and deforestation activities were also important factors for vegetation browning in local areas (Kumar et al., 2010; Buyantuyev and Wu., 2012; Du et al., 2019).

Terrestrial ecosystems of China are important to global carbon balance because of rich diversity and large area (Piao et al., 2009). Change in the vegetation is one key factor affecting carbon sink/source function. Therefore, understanding the spatial-temporal variation of terrestrial vegetation and their driving forces in China is necessary. The observed records shown that the surface temperature increased by 1.1 °C since 1950s, which was more obvious than many regions in Northern Hemisphere. Although the increase trend of precipitation was not significant for the whole China, but change was different in diverse regions (Yuan et al., 2017). Besides, mainland China has experienced rapid urbanization in recent several decades (Deng et al., 2015). It was observed that the urban area in mainland China increased by 6.11×10^4 km^2 from the late 1980s to mid-2010 (Li et al., 2018). As a result of land use change and population increase, nearly 90% of grasslands in China have been degraded (Wang et al., 2016). It was reported that approximately 9 million hm^2 of newly forestland and grassland were converted from cultivated land and about 14 million hm^2 of unused land was afforested by the late 2000s (Chen et al., 2009). Changes in these driving factors of vegetation growth led to restoration or degradation. But the extent of impact caused by climate change and human activities is still ambiguous. The research carried by Shi et al. (2020) showed that human activities is the definitive factor for greening in China, with contribution proportion more than 100% in most regions. While Zhang et al. (2020) found that in more than half area of the Yangtze River and Yellow River Basin, the influence of climate change on vegetation was greater than that of human activities.

This research took the China as the study area and explored the effects of climatic and anthropogenic environmental factors on EVI variation. The changes of precipitation and temperature were selected as the mainly climatic environmental factors. While for the anthropogenic environmental factors, we discussed the effects of urbanization, cultivation and afforestation by using nighttime lights data, land use/land cover data and other record data from China Statistical Yearbook. We addressed the following key issues: (i) analyze spatial-temporal variation of EVI in mainland China; (ii) explore the relationship between vegetation growth and different driving forces; (iii) distinguish and quantify the contribution of different driving forces to the change in EVI. The remaining sections of this paper were organized as follows: the study area and datasets were introduced in Section 2; Section 3 described the methodologies used in this study. The analysis results were shown in Section 4. And the discussion and conclusions were summarized in Section 5 and 6 respectively.

2. Study Area and Data

2.1. Study Area

China (Latitude: 3°51′ N to 53°33′ N; Longitude: 73°33′ E to 135°05′ E) locates in the Northern Hemisphere subtropical and mid-latitude area, covering an area of 9.63 million km^2 (Figure 1). The elevation of mainland China decreases from

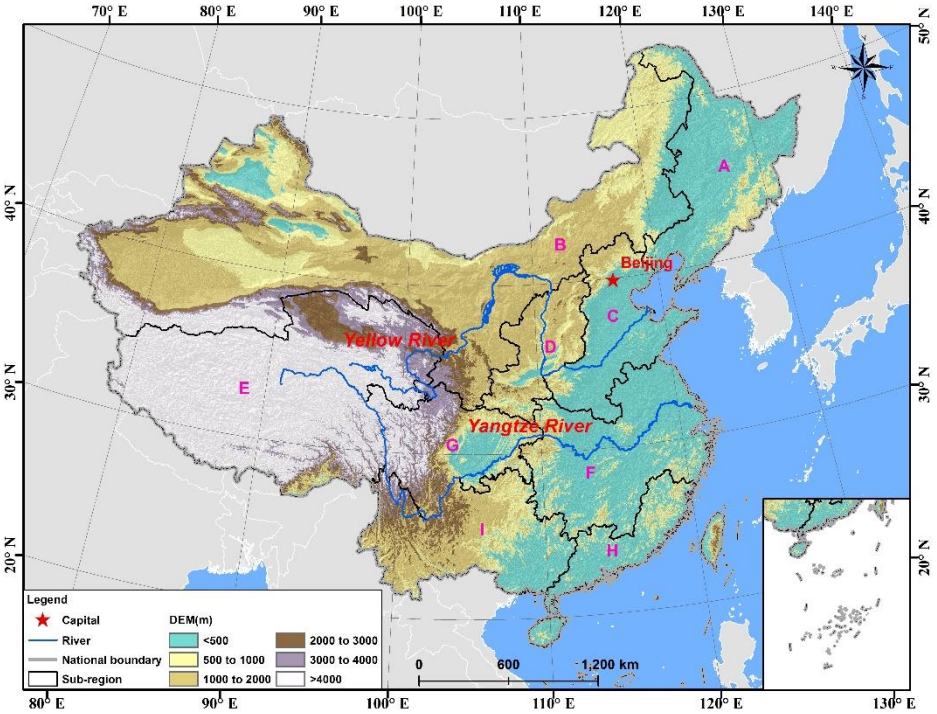

Figure 1. The location of China.

more than 5,000 m in west to less than 10 m in east, with a three-ladder-like distribution. The country has five main climate zones, namely, temperate monsoon, subtropical monsoon, tropical monsoon, plateau mountain, and temperate continental (Wang et al., 2017). The average annual precipitation is about 300 to 1200 mm from north to south, with a spatial average of 643 mm (Yuan et al., 2017). The average annual temperature ranges from −16 to 26 °C with a spatial average around 10 °C (Yang et al., 2020). The land cover in the mainland China consists primarily of grassland (31.6%) and forestland (23.4%). Water area and construction land are less dominant land cover types, accounting for 2.9 and 2.3% of the total area. The vegetation in China changes among regions greatly. The type of vegetation includes: evergreen broadleaf forest, deciduous broadleaf forest, mixed forest, woody savannas, croplands, grasslands and shrublands. According to the study carried by Xu et al. (2002), we divided mainland China into nine regions, including Northeast China Plain (Region A, NCP), Northern arid and semiarid region (Region B, NASR), Huang-Huai-Hai Plain (Region C, HHHP), Loess Plateau (Region D, LP), Qinghai-Tibet Plateau (Region E, QTP), Middle-lower Yangtze Plain (Region F, MLYR); Sichuan Basin and surrounding regions (Region G, SBSR), Southern China (Region H, SC) and Yunnan-Guizhou Plateau (Region I, YGP). The shapefile of these nine regions' boundary can be download from Resource and Environment Science and Data Center (RESDC, http://www.resdc.cn/).

2.2. Datasets

2.2.1. EVI Data

Spatial-temporal variation of vegetation coverage can be quantified by EVI. In this research, the EVI data was obtained from global monthly MOD13A3 products (version: 006), which was available from https://earthdata.nasa.gov/. The data was in HDF format covering 2000 to 2019 and 1 km spatial resolution. With Maximum Value Composite (MVC) approach and ArcGIS 10.3 software, the annual EVI for the mainland China was derived (Figure 2(a)). The value of EVI is between −0.2 and 0.05 for snow, inland water bodies, bare soil, sparse vegetation and other non-vegetated areas. In this study, we selected the areas with EVI ≥ 0.05 as the vegetated land (Wang et al., 2013).

2.2.2. Meteorological Data

The gridded meteorological data during 2000 to 2019 was obtained from China Ground Precipitation 0.5° × 0.5° Grid Dataset V2.0 and China Ground Temperature 0.5° × 0.5° Grid Dataset V2.0, which are provided by National Meteorological Information Center (NMIC, http://data.cma.cn/). These datasets (a total of 3,825 grids) were based on the daily observation from 2,474 national meteorological stations and generated by thin plate spline and the GTOPO30 (Global 30 arc-second elevation) DEM data (Figure 2(b)). The gridded data has been projected and resampled in order to ensure the same coordinate system and resolution (1 km × 1 km) with MOD13A3 products.

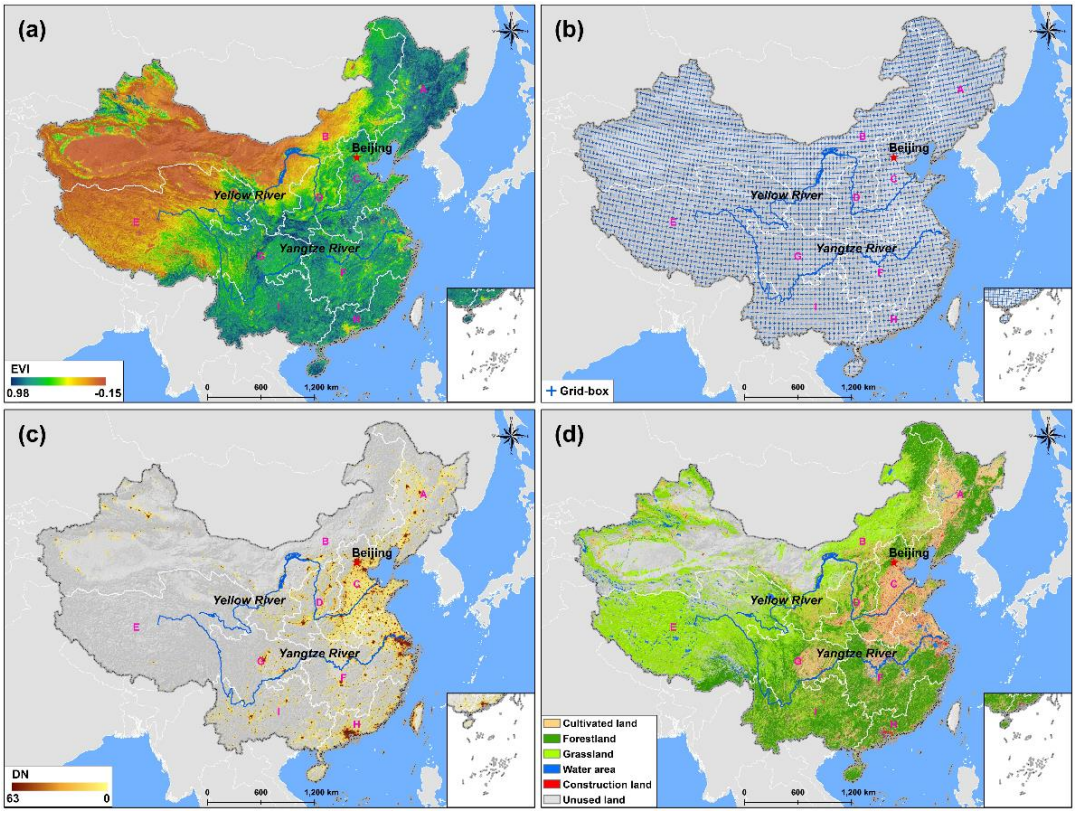

Figure 2. The datasets used in this study. (a) EVI data (take 2019 year as example); (b) Box-points for meteorological data; (c) DMSP-OLS data (take 2013 year as example); (d) LULC data (take 2015 year as example).

2.2.3. Nighttime Lights Data

Defense Meteorological Satellite Program (DMSP) Operational Linescan System (OLS) dataset is widely used as an indicator of human activity. The radiance in each pixel is qualified by a Digital Number (DN) value ranging from 0 to 63 (Figure 2(c)). A higher value indicates more lights emitted by cities and more human activities. The DMSP-OLS global stable light images from 2000 to 2013 can be download from RESDC (http://www.resdc.cn/). Nighttime lights data of mainland China was extracted and projected by ArcGIS 10.3 software in order to ensure the same coordinate system with EVI data. Although the timespan of DMSP-OLS dataset is seven years shorter than that of EVI dataset, the results still make sense in the context of rapid urbanization.

2.2.4. Land Use/Land Cover Data

Land use/land cover (LULC) data with a spatial resolution of 1 km × 1 km for the years 2000 and 2015 was obtained from RESDC (http://www.resdc.cn/). This dataset is generated by remote sensing images with manual visual interpretation method. The quality has been controlled and integration has been checked by RESDC. The types of LULC were divided into six categories in this study, including cultivated land, forestland, grassland, water area, construction land and unused land (Figure 2(d)). Comparing the land use/land cover maps for 2000 and 2015, the expanded construction land can be obtained.

2.2.5. Statistical Data from National Bureau of Statistics of China

Annual statistical data about forest area, accumulated afforested area, forest coverage, harvested area, total food production, effective irrigation area and amount of fertilizer use can be obtained from National Bureau of Statistics of China (NBSC, http://www.stats.gov.cn/). Statistical data about forest (e.g., forest area and coverage rate, afforestation) covered the period 2004 to 2018. Statistical data about cultivated land (e.g., harvested area, total food production, effective irrigation area and amount of fertilizer) covered the period 2000 to 2018.

3. Methodology

In this study, the linear regression and moving *t*-test were used to investigate the vegetation trend and abrupt change, in both region scale and pixel scale. Then these spatial-temporal variations were discussed in regard to climate factors and human activities. For climate factors, precipitation and temperature were selected as the main factors influenced the EVI change. For human activities, we focused on the urbanization, cultivation and afforestation. Finally, the impacts of climate change and human activities on vegetation variation were quantified by Residual trend (RESTREND) analysis (Figure 3).

3.1. Trend Analysis of EVI and Climatic Factors

3.1.1. Linear Regression and the Slope

To identify the inter-annual trend of variable, the linear regression method was adopted to eliminate the increase or decrease rate of EVI and climatic factors (Tian et al., 2019), which can be calculated as follows:

$$Slope = \frac{n \times \sum_{i=1}^{n}(i \times x_i) - \sum_{i=1}^{n} i \sum_{i=1}^{n} x_i}{n \times \sum_{i=1}^{n} i^2 - (\sum_{i=1}^{n} i)^2} \quad (1)$$

where *Slope* is the linear slope of the time series variable, which can be used to characterize the increase or decrease rate during a given study period; n is the number of years; x_i is the value of variable for the i^{th} year (i = 1, 2, …, n).

The *F*-test was used to test the significance of trend of variable, and *F*-value can be calculated as follow:

$$F = \frac{(n-2) \times \sum_{i=1}^{n}(x_i - \bar{x})^2}{\sum_{i=1}^{n}(x_i - x_i)^2} \quad (2)$$

where x_i is the regression value of variable in i years and $\bar{x}$ is the average value of variable for a given period.

3.1.2. Abrupt Change Detection by Moving *t*-Test

Moving *t*-Test is one of widely used methods for abrupt change detection, which tests a hypothesis based on a difference between sample means. For the time series (x_i, i = 1, 2, …, n), the statistic values (t) can be calculated as Equations (3) and (4):

$$t = \frac{(\bar{x}_1 - \bar{x}_2)}{s\sqrt{\frac{1}{n_1} + \frac{1}{n_2}}} \quad (3)$$

$$s = \sqrt{\frac{n_1 s_1^2 + n_2 s_2^2}{n_1 + n_2 - 2}} \quad (4)$$

where $\bar{x}_1(\bar{x}_2)$, $s_1(s_2)$ and $n_1(n_2)$ are the average value, standard deviation and length a subsequences. In this research, $n_1 = n_2 = 5$. Given a significant level α, if $|t_i| > t_\alpha$, the point (i^{th} year) could be regarded as abrupt change point for the time series (EVI or climatic factors).

3.2. Correlation Analysis and Identification of Dominate Climate Factors

3.2.1. Partial Correlation Coefficient and Multiple Correlation Coefficient

To assess the effects of precipitation and temperature on EVI in mainland China, Multiple correlation coefficient ($R_{z,xy}$) and partial correlation coefficient ($r_{zx,y}$ or $r_{zy,x}$) were employed to analyze the correlation between EVI and major climatic factors (Yin et al., 2020). These two kinds of coefficients can be calculated as follows:

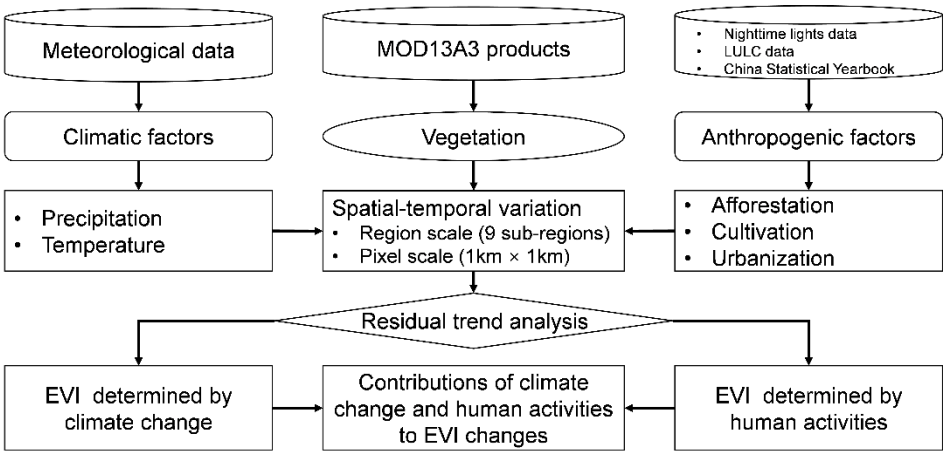

Figure 3. The flowchart of the investigation of vegetation change.

① Partial Correlation Coefficient

$$r_{zx,\,y} = \frac{r_{zx} - r_{zy} - r_{xy}}{\sqrt{(1 - r_{zy})(1 - r_{xy})}} \tag{5}$$

where $r_{zx,\,y}$ denotes the partial correlation coefficient of variable x and variable z, holding variable y constant. r_{zx}, r_{zy}, r_{xy} denotes correlation coefficients of variables x and z, y and z, and x and y respectively. The partial correlation coefficient can be used for quantifying relationship between EVI and precipitation or relationship between EVI and temperature. The significance of partial correlation was estimated by t-test. Test statistic t defined as:

$$t = \frac{r_{zx,\,y}}{\sqrt{1 - r_{zx,\,y}^2}}\sqrt{n - m - 1} \tag{6}$$

where n and m are number of samples and the number of independent variables, respectively:

② Multiple Correlation Coefficient

$$R_{z,\,xy} = \sqrt{1 - (1 - r_{zx}^2)(1 - r_{zy,\,x}^2)} \tag{7}$$

where $R_{z,\,xy}$ denotes the multiple correlation coefficient of dependent variable z and independent variable x and y. The multiple correlation coefficient can be used for quantifying relationship between EVI and precipitation or relationship between EVI and climatic factors. The significance of multiple correlation was estimated by F-test. Test statistic F defined as:

$$F = \frac{R_{z,\,xy}^2}{1 - R_{z,\,xy}^2} \times \frac{n - k - 1}{k} \tag{8}$$

where n and k are number of samples and the number of independent variables, respectively.

3.2.2. Identifying Climatic Factors on EVI Changes

The dominant climate factors affecting the changes in EVI can be identified based on the correlation analysis mentioned above. According to the previous studies carried by Yin et al. (2020), the dominant climate factors were divided into four categories. Classification criteria was illustrated in Table 1. FCLI is the statistic F of multiple correlation between EVI and major climatic factors; t_{PRE} (t_{TEM}) is the statistic t of partial correlation between precipitation (temperature) and EVI.

3.3. Contribution Analysis of Different Driving Forces to the Change in EVI

3.3.1. Residual Trend (RESTREND) Analysis

For a given region and period, the vegetation growth is influenced by both climatic and anthropogenic factors. We can decompose observed EVI into two parts, namely EVI determined by climate and EVI determined by human activities, which can be written as:

$$EVI_i = EVI_{c,i} + EVI_{h,i} \tag{9}$$

where EVI_i is observed EVI value for t-year; $EVI_{c,\,i}$ and $EVI_{h,\,i}$ represent EVI determined by climate and EVI determined by human activities respectively. $EVI_{c,\,i}$ can be predicted by Multivariate Linear Regression (MLR) and $EVI_{h,\,i}$ can be identified after removing the climate influence (Herrmann et al., 2005; Wessels et al., 2007):

$$EVI_{c,i} = f(PRE_i, TEM_i) \tag{10}$$

$$EVI_{h,\,i} = EVI_i - f(PRE_i, TEM_i) \tag{11}$$

where $f(PRE_i, TEM_i)$ is EVI estimated from climate factors, e.g., precipitation and temperature.

3.3.2. Contribution Calculation of Driving Forces

Based on Equation (1), a positive *Slope* in EVI represents

vegetated lands showing greening, whereas a negative *Slope* denotes vegetated lands showing browning. Thus, six possible scenarios, including vegetated lands greening/browning caused by climate change (CC), vegetated lands greening/browning caused by human activities (HA), and vegetated lands greening/browning caused by both CC and HA. Contribution proportions of driving forces in these six scenarios can be quantified according to Table 2.

4. Results

4.1. Spatial Pattern of Multi-Year Average EVI

With the 20-year (2000 to 2019) EVI dataset, the spatial pattern of average EVI was calculated and showed in Figure 4. Over the entire mainland China, the average EVI ranged from 0.05 to 0.88 with an average value of 0.38 from 2000 to 2019. In general, the EVI is lower in the northwest and increases toward the southeast. The EVI was normally lower than 0.30 in the Northwest China, where barren land is widely distributed. The precipitation is less and/or temperature is lower, which are not favorable to vegetation growth. However, the EVI in most southern China is higher than 0.50. This area is characterized by warmer and wetter climate and plenty evergreen forests.

Based on the spatial distribution of average EVI, the relationship between EVI and geographical factors (longitude, latitude and elevation) was illustrated in Figure 5. A significantly increasing rate of EVI as the longitude increased can be observed, defining a green rate of 0.009 per degree in longitude (Figure 5(a)). Between 15° E to 40° E, the EVI decreases by 0.019 per degree in latitude. However, the EVI increases with rising latitude by 0.025 per degree between 40° E to 55° E (Figure 5(b)). When the elevation is less than 3,500 m, EVI is less sensitive to the change of elevation. The EVI reduces by 0.005 as the elevation increases by every 100 m. When the elevation is more than 3,500 m, EVI is more sensitive to the change of elevation. A 100 m increase in elevation leads to a decrease of about 0.01 in EVI (Figure 5(c)).

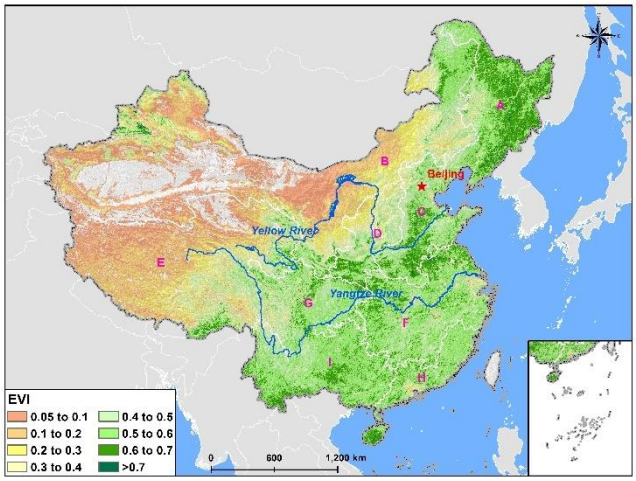

Figure 4. The average EVI during period 2000 to 2019. (*Note: the grey areas filled with grey color represent non-vegetated areas (EVI < 0.05)).

4.2. Spatial-Temporal Variation of EVI

4.2.1. Interannual Variations of EVI

Figure 6 illustrated the interannual variation of EVI at the entire mainland China, showing a significant increase trend from 2000 to 2019 (*Slope* = 0.002/yr, $p < 0.05$). A break point in 2009 can be detected by moving *t*-test. The increasing rates were 0.0028/yr ($p < 0.05$) and 0.0013/yr ($p < 0.05$) for period 2000 to 2009 and period 2010 to 2019 respectively, indicating a relatively weak positive trend in recent 10 years. The multi-year average EVI was 0.393 after 2009, increasing by 6.3% compared with that before 2009.

Table 1. Classification Criteria for Dominant Climate Factors Identification

Driving factors		Criteria
Precipitation		$F_{CLI} < F_{0.1}$, $t_{PRE} < 0.05$, $t_{TEM} \geq 0.05$
Temperature		$F_{CLI} < F_{0.1}$, $t_{PRE} \geq 0.05$, $t_{TEM} < 0.05$
Driving of temperature and precipitation	Weak	$F_{CLI} < F_{0.1}$, $t_{PRE} \geq 0.05$, $t_{TEM} > 0.05$
	Strong	$F_{CLI} < F_{0.1}$, $t_{PRE} < 0.05$, $t_{TEM} < 0.05$

Table 2. Contribution Calculation of Driving Forces to the Change in EVI

Scenarios	*Slope* *EVI*	EVI_c	EVI_h	Contribution proportion (%) CC	HA
Greening caused by CC and HA (GCH)	> 0	> 0	> 0	$\frac{Slope(EVI_c)}{Slope(EVI)}$	$\frac{Slope(EVI_h)}{Slope(EVI)}$
Greening caused by CC (GC)	> 0	> 0	< 0	100	0
Greening caused by HA (GH)	> 0	< 0	> 0	0	100
Browning caused by CC and HA (BCH)	< 0	< 0	< 0	$\frac{Slope(EVI_c)}{Slope(EVI)}$	$\frac{Slope(EVI_h)}{Slope(EVI)}$
Browning caused by CC (BC)	< 0	< 0	> 0	100	0
Browning caused by HA (BH)	< 0	> 0	< 0	0	100

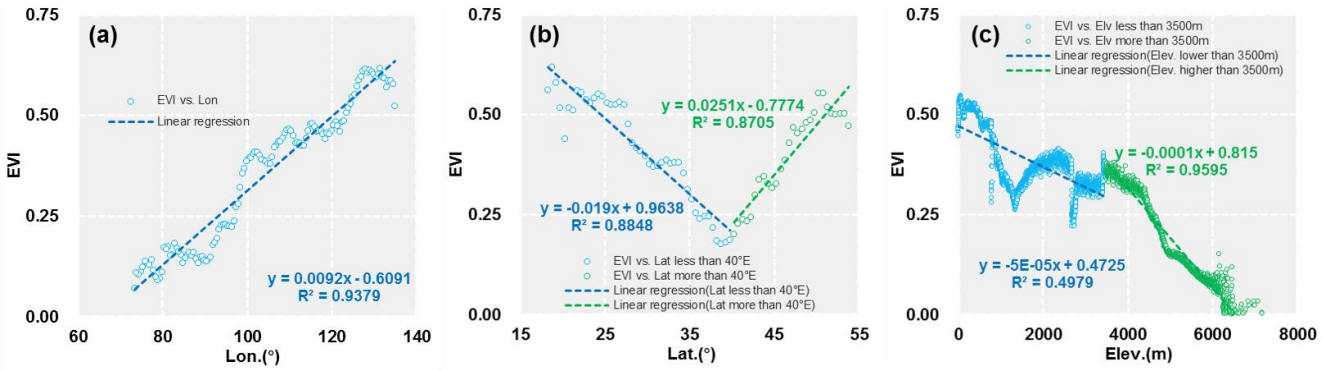

Figure 5. The relationship between average EVI and longitude (a), latitude (b) and elevation(c).

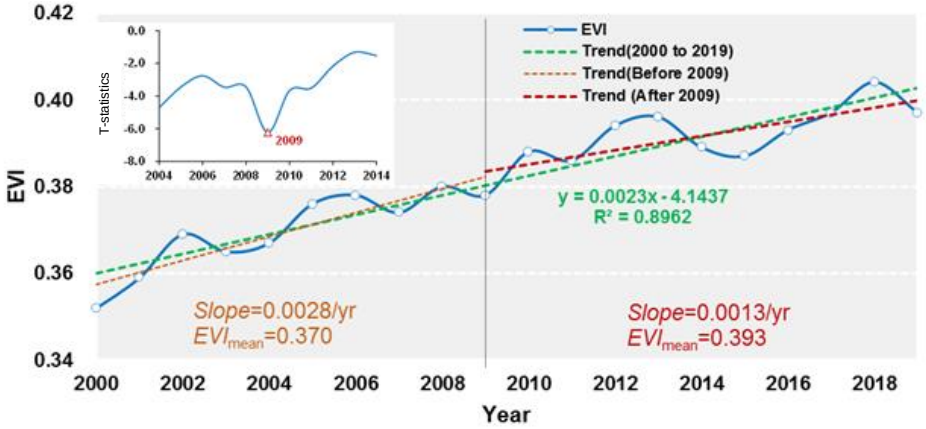

Figure 6. Interannual variation of EVI from 2000 to 2019. The small inset figure shows the moving *t*-Test result of EVI series.

Table 3. The Breakpoint and Slope of Spatial Average EVI Curve for Each Sub-Rregion

Region	Breakpoint	Muti-year average EVI			Slope (EVI unit per year)		
		Phase 1 (before breakpoint year)	Phase 2 (after breakpoint year)	2000 to 2019	Phase 1 (before breakpoint year)	Phase 2 (after breakpoint year)	2000 to 2019
NCP	2009	0.545	0.583	0.564	0.0044*	0.0010	0.0035*
NASR	2010	0.231	0.255	0.242	0.0014	0.0019	0.0022*
HHHP	2004	0.490	0.521	0.513	0.0115*	−0.0002	0.0018*
LP	2011	0.411	0.465	0.433	0.0065*	0.0012	0.0054*
QTP	2008	0.226	0.232	0.229	0.0002	0.0002	0.0006*
MLYR	2004	0.512	0.538	0.527	0.0048*	−0.0001	0.0023*
SBSR	2008	0.478	0.498	0.493	0.0008	0.0018*	0.0019*
SC	2004	0.501	0.541	0.529	0.0027	0.0031*	0.0037*
YGP	2005	0.516	0.552	0.543	0.0020	0.0024*	0.0031*

Note: * means the trend is significant with $p < 0.05$.

The breakpoint and slope for each sub-region was list in Table 3. It can be concluded that spatial average EVI for each sub-region increased during period 2000 to 2019, with a rate of 0.0005 to 0.0054 per year. Each of the sub-basins showed a significant increase ($\alpha = 0.05$) in EVI during study period. The green rate of LP is the highest among all the sub-regions. It is mainly because a series of ecological construction and protection projects has been implanted since 1999. And plenty cultivated land has been returned to forestland or grassland (Xie et al., 2014; Li and Wang, 2019). The breakpoints of most sub-regions occurred at the late 2000s and early 2010s. The spatial average values of EVI in Phase 2 (after breakpoint) increased by 3.0 to 13.2% compared with those in Phase 1 (before breakpoint). In NCP and LP, the increasing rate was slower in Phase 2 than that in Phase 1. While opposite change character showed in NASR, SBSR, YGP and SC. In HHHP and MLYR, the EVI showed a decreasing-to-increasing trend, which is different from the consistent increasing trend detected in other sub-regions.

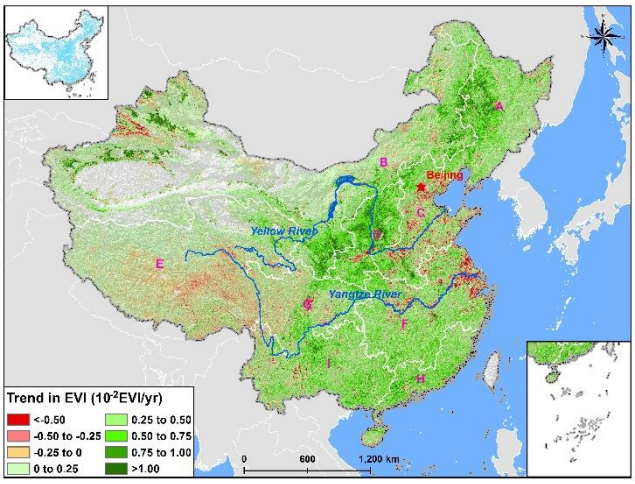

Figure 7. Spatial distribution of the trend in EVI. The small inset figure shows spatial pattern of trend significance levels. The region filled in blue is significant at $p < 0.05$.

4.2.2. Spatial Distribution of EVI Trends

The trends (slope) of EVI from 2000 to 2019 differed spatially throughout mainland China (Figure 7). The slight decreasing trend ($-0.0025 \leq Slope < 0$) is mainly concentrated in QTP and SBSR, especially in Tibet, southern Qinghai and Western Sichuan. The sharp decreasing trend ($Slope < -0.005$) is scattered in HHHP and Yangtze River Delta, which characterized by rapid economic development and urbanization. The EVI increased in 82.8% of the study area, and the significant increasing trend ($p < 0.05$) accounted for 42.1% of the vegetated land. In contrast, about 17.2% of the area showed a decreasing trend. The area with a significant decreasing trend ($p < 0.05$) in EVI accounted for 2.7% of the total area. Create Random Points Tool provided by ArcGIS 10.3 software was used to randomly select 50,000 pixels from all the pixels in vegetated land in mainland China (a total of 8,494,651 pixels, resolution of each pixel is 1 km × 1 km). The break point of EVI series in each pixel was detected by Moving *t*-test. Then period 2000 to 2019 was divided in Phase 1 (before break point) and Phase 2 (after break point). There were 26,703 pixels whose EVI series had break point. The EVI trends of these 26,703 pixels for Phase 1 and Phase 2 was compared by Figure 8. EVI in 32.4% of the points exhibited consistent increasing trend in both Phase 1 and Phase 2. In contrast, approximately 20.6% of the points showed consistent decreasing trend in these two phases. The EVI increasing-to-decreasing trend and decreasing-to-increasing trend accounted for 27.9 and 19.1% of the points, respectively (Figure 8(a)). In addition, about 44.8% of the points had a lower change rate in Phase 2, with a lower absolute slope value than Phase 1. This statistic indicated that vegetation experienced slower greening or degradation in Phase 2 (Figure 8(b)).

4.3. Relationship between EVI and Climate Change

4.3.1. Spatial-Temporal Variation of Precipitation and Temperature

The trends of precipitation and temperature over the whole study area were illustrated in Figure 9. The annual precipitation decreased from 631.5 mm in 2000 to 594.5 mm in 2009. Then it showed an increase trend with some fluctuation and reach to 628.4 mm in 2019, indicating a decreasing-to-increasing trend (Figure 9(a)). A consistent increasing trend of annual average temperature can be detected in Figure 9(b). The temperature for the whole study area rose at a rate of 0.05 °C/yr during period 2000 to 2009 and 0.08 °C/yr during period 2010 to 2019. The wetter and warmer climate in recent years might be an important driver for the greener vegetation.

As indicated in the spatial trend distribution map (Figure 10), the positive precipitation changes mainly be found in Most of China, especially in NCP and MLYR. While southern HHHP and western YGP have witnessed less precipitation in recent two decades. Previous research also detected that these two

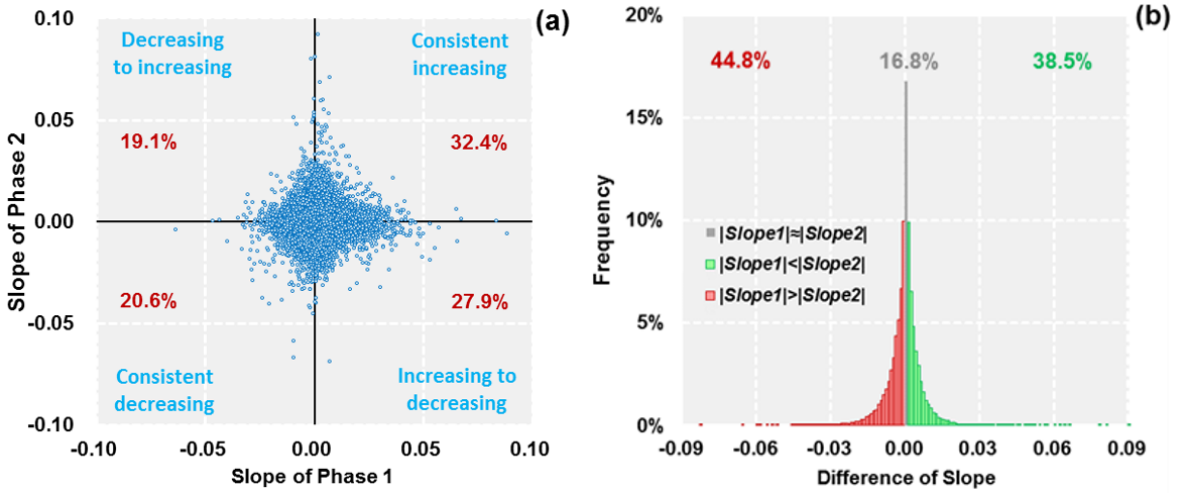

Figure 8. Scatter-plot for EVI slope (a) and histogram for difference of absolute slope value (b) (Note: for subfigure (a), percentage number means the proportion of points in corresponding quadrant).

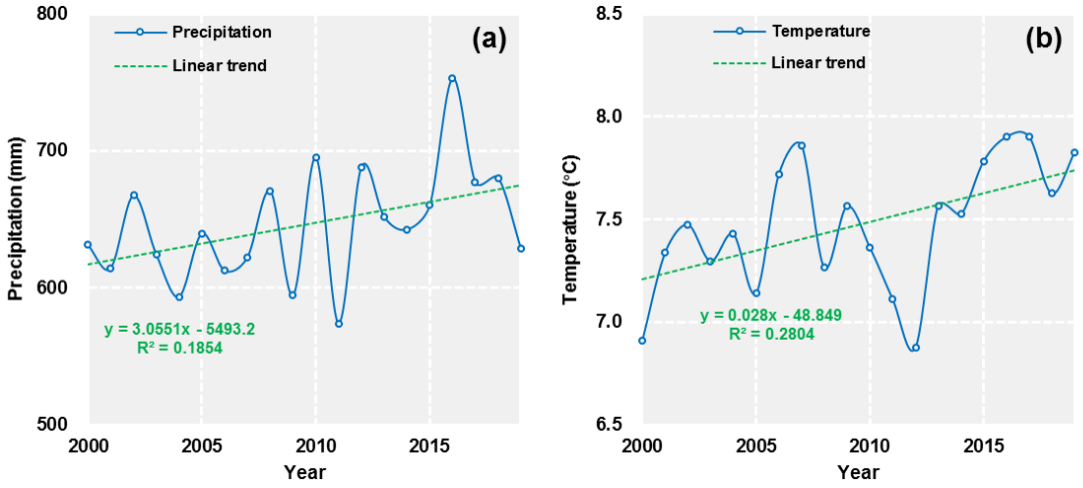

Figure 9. Interannual variation of precipitation (a) and temperature (b) from 2000 to 2019.

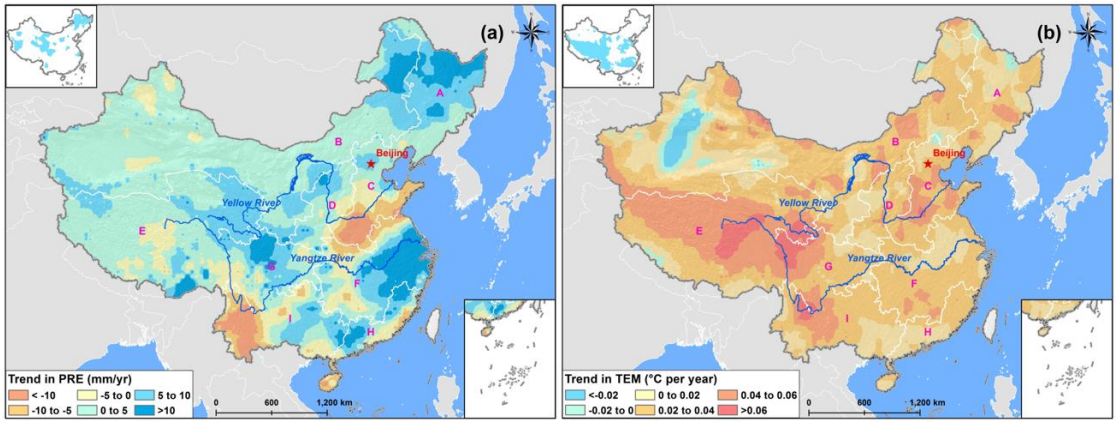

Figure 10. Spatial distribution of the trends in precipitation (a) and temperature (b). The small inset figures show spatial pattern of trend significance levels. The region filled in blue is significant at $p < 0.05$.

regions were suffered from frequent droughts since 2000s (Yuan et al., 2015; Yuan et al., 2017). Areas with significantly positive trend and negative trend ($p < 0.05$) accounted for 21.2 and 0.9% of the total respectively, indicating precipitation trends in most of mainland China were non-significant (Figure 10(a)). Increasing temperature trends were observed over 96.1% of mainland China during 2000 to 2019. Area with significant increase trend ($p < 0.05$) accounted for 36.7% of the total area, which were mainly located in the QTP, HHHP and MLYR (Figure 10(b)).

4.3.2. EVI Changes Related to Major Climatic Factors

The response of EVI to major climatic factors was explored by multiple linear regression. The multiple correlation coefficients were illustrated in Figure 11(a). Areas with high multiple correlation coefficients mainly distributed in northern China, indicating the higher climate contributions to vegetation growth in these regions. Partial correlation between EVI and climate factors was showed in Figure 11(b) and Figure 11(c). The EVI was positively correlated with precipitation in majority pixels (73.2%, with significant correlation coefficients in 18.6% of pixels), which were mainly distributed in Inner Mongolia and Qinghai Province. The significant negative correlation (only 1.3%) primarily occurred in Anhui Province and Jiangsu Province (Figure 11(b)). Area with positive correlation between EVI and temperature accounted for 63.4% of the study area. And the significant positive correlation (6.7% of the study area) was mainly observed in QTP. Pixels with significant negative correlation only accounted for 1.8% and scattered in HHHP (Figure 11(c)). Dominant climatic factors affecting EVI in vegetated lands during period 2000 to 2019 were showed in Figure 11(d). Areas with EVI significantly affected by climate factors ($p < 0.1$) accounted for 15.0% of the vegetated lands. Areas dominated by precipitation accounted for 63.5% of the total significant region, widely distributing in NASR (especially Inner Mongolia) and QTP (especially Qinghai Province). While areas dominated by temperature accounted for 7.7% of the total significant region, mainly distributed in MLYR (especially Jiangxi Province). About 28.8% of the total significant areas were dominated by both temperature and precipitation, mainly distributing in QTP.

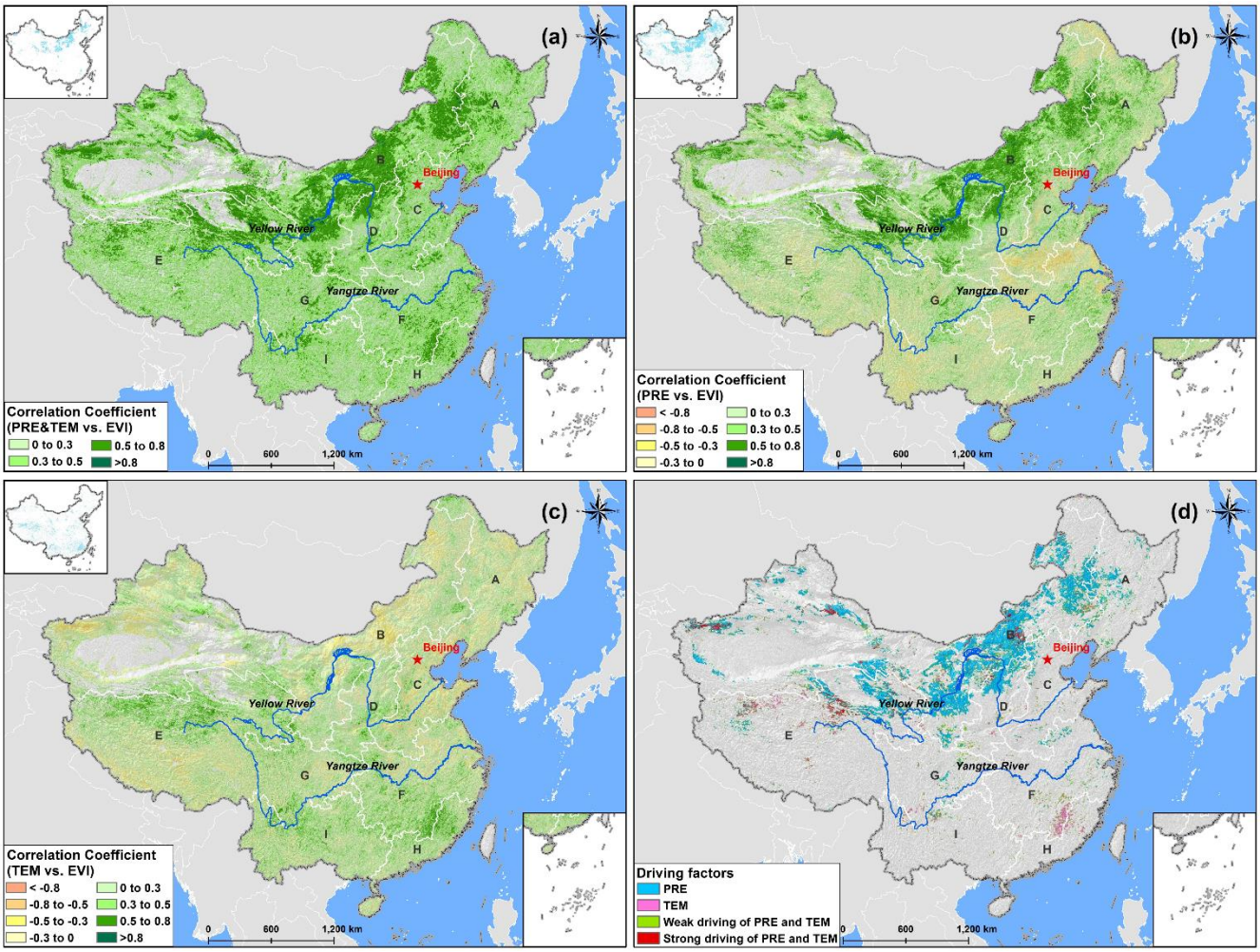

Figure 11. Spatial distribution of correlation coefficient between EVI and major climatic factors and driving factors: (a) Multiple correlation coefficient; (b) Partial correlation coefficient between EVI and precipitation; (c) Partial correlation coefficient between EVI and temperature; (d) Climate factors significantly affecting EVI. The small inset figures in (a) to (c) show spatial pattern of correlation significance levels. The region filled in blue is significant at $p < 0.05$.

Table 4. Correlation of EVI with Climate Factors over the Period 2000 to 2019

Region	NCP	NASR	HHHP	LP	QTP	MLYR	SBSR	SC	YGP	China
EVI vs. PRE&TEM	0.603**	0.859**	0.091	0.460	0.526*	0.62**	0.521**	0.597**	0.359	0.580**
EVI vs. PRE	0.555**	0.856**	0.077	0.285	0.396*	0.237	0.289	0.049	0.129	0.476**
EVI vs. TEM	0.050	0.119	0.012	0.297	0.443*	0.571**	0.450**	0.583**	0.335	0.424*

Note: * means the trend is significant with p < 0.1; ** means the trend is significant with $p < 0.05$.

The relationship between EVI and major climatic factors over the period 2000 to 2019 in nine sub-regions and the entire mainland China were also analyzed (Table 4). The spatial average EVI in mainland China had significant positive correlation with climatic factors (REVI-PRE&TEM = 0.580, $p < 0.05$). And precipitation was more influential for the vegetation growth in mainland China. However, EVI's response to climatic variations was different for different sub-regions. It can be seen from Table 4 that for NCP and NASR, EVI correlated significantly with precipitation. All these two sub-regions located in northern China, with limited rainfall resource. Thus, the vegetation is more sensitive to precipitation. In contrast, EVI correlated strongly with temperature in MLYR, SBSR and SC, where is located in southern China. Vegetation growth is restricted by thermal conditions. In QTP, both precipitation and temperature affected vegetation growth significantly.

4.4. Relationship between EVI and Human Activities

4.4.1. EVI Changes Related to Urbanization

The distribution of annual nighttime light trends (slope) was illustrated in Figure 12. Area exhibited significant increas-

ing DN trend (α = 0.05) accounted for 13.3% of mainland China. The spatial distribution of the trend in DN indicated the ongoing urbanization in China since 2001, especially in HHHP, Yangtze River Delta of MLYR and SC. The scatterplot of significant EVI trend and significant DN trend were generated and illustrated in Figure 13. About 73.8% of the points showed both increasing trends in EVI and DN (Quadrant I), that is to say most vegetation still grew well during the urbanization period. But we can find that the faster greening rate were found in the area with slower urbanization. Approximately 26.1% of the point showed increasing EVI and decreasing DN (Quadrant II) or decreasing EVI and increasing DN (Quadrant IV), indicating the negative effects of urbanization. Only 0.1% of the points showed both decreasing trends in EVI and DN (Quadrant III), probably due to timber production (Figure 13).

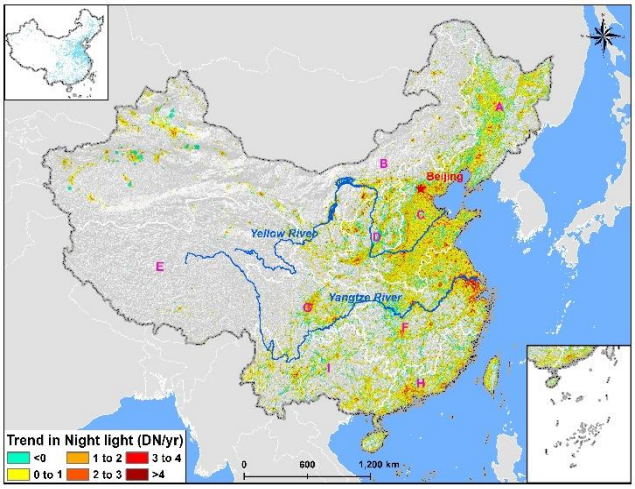

Figure 12. Spatial distribution of the trend in DN. The small inset figure shows spatial pattern of trend significance levels. The region filled in blue is significant at $p < 0.05$.

The spatial distribution of the trend in DN (Figure 12) indicated a rapid urbanization in China since 2000. According to land use/land cover maps, the construction land in mainland China has expanded from 1.70×10^5 km^2 in 2000 to 2.18×10^5 km^2 in 2015, with an average annual growth rate of 1.67%. The shrinks of cultivated land, forestland and grassland contributed to 66.4, 12.6 and 10.7% of urban expansion, respectively. It can be concluded that urban expansion has led to a massive loss of cultivated lands in mainland China. The expanded construction land was primarily concentrated HHHP, MLYR and SC (Figure 14), which coincided with research carried by Li et al. (2018). Areas with significant EVI decrease were 4.67×10^4, 6.86×10^4 and 1.22×10^4 km^2 for HHHP, MLYR and SC respectively. And it was clear in the Figure 14 that these areas mainly located in the construction land, especially the new expended construction land. During the urbanization process, plenty vegetation covers has been replaced by impervious surfaces, leading to the reduction in EVI. Similarly, the expand of construction land in HHHP, MLYR and SC was mainly caused by the decrease of cultivated land. In HHHP, MLYR and SC, about 6.57×10^3, 12.27×10^3 and 3.47×10^3 km^2 of the original cultivated land have been turned into construction land, which were 83.1, 78.7 and 55.2% of the newly increased construction land. In regions where cultivated land was turned into construction land, the EVI change rates were -0.405×10^{-2}, -0.415×10^{-2} and -0.006×10^{-2}/yr in HHHP, MLYR and SC, respectively.

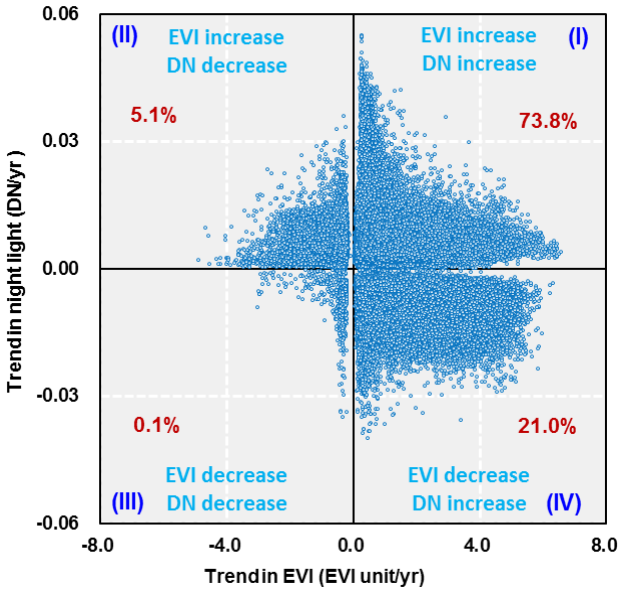

Figure 13. Scatterplot of EVI trends ($p < 0.05$) and DN trends ($p < 0.05$).

4.4.2. EVI Changes Related to Forests and Croplands

Statistical data of annual forest and croplands in China was showed in Tables 5 and 6, which was provided by National Bureau of Statistics of China (https://data.stats.gov.cn/). In recent 10 years, the forest area has increased by 19.6%, mostly as a result of expanding natural forests and afforestation. The greening trends in forest benefit from several programs, such as Three North Shelterbelt Development Program, Beijing-Tianjin Sand Source Control Program, Natural Forest Conservation Program and Grain to Green Program (Zhang et al., 2016). Accumulated afforested area was 70.40×10^6 hm^2 for the period 2009 to 2018, accounting for about a third of current forest area. It could be found that China had comparable and stable harvested area in recent 10 years. The multi-year average harvested area was 163.31×10^6 hm^2 after 2009, increasing by only 5.8% compared with that before 2009. While the statistical data revealed a 31.2% increase in total food production in a single decade due to in equal measure from and irrigation and heavy fertilizer use. Effective irrigation area and amount of fertilizer use had increased by 16.2 and 24.7% in recent 10 years. The spatial forest coverage rate and total food production were illustrated in Figure 15. It could be found that NCP, LP and YGP experienced massive forestation in recent years. While the total food production in NASR and HHHP increased significantly, which led to the cropland greening. These is reflected in the spatial distribution of EVI trends showed in Figure 7.

4.5. Influence of Climate Change and Human Activities on Vegetation Dynamics

4.5.1. Spatial Distribution of EVI_c and EVI_h Trends

The regions where EVI show significant trends (RST) were selected for analysis of drivers. The trends (slope) of EVI_c and EVI_h during 2000 to 2019 differed spatially throughout the RST (Figure 16). EVI_c increased in most of the RST (accounting for 89.8%). The area with a moderate increase trend (0.0025 per year ≤ *Slope* < 0.005 per year) of EVI_c covered 8.3% of the RST and was concentrated in NCP and eastern TP (e.g., Qinghai Province). Whereas only 0.1% of the RST experienced large increase trend of EVI_c (*Slope* ≥ 0.005 per year) (Figure 16(a)). However, EVI_h showed more intensive variation than EVI_c throughout the RST. Nearly 50% of the RST exhibited moderate or large increasing tendency of EVI_h (*Slope* ≥ 0.0025 per year). The area with a large increase trend was concentrated in LP. While the areas that exhibited decreases in EVI_h showed a discrete geographical distribution in HHHP and MLYR (Figure 16(b)).

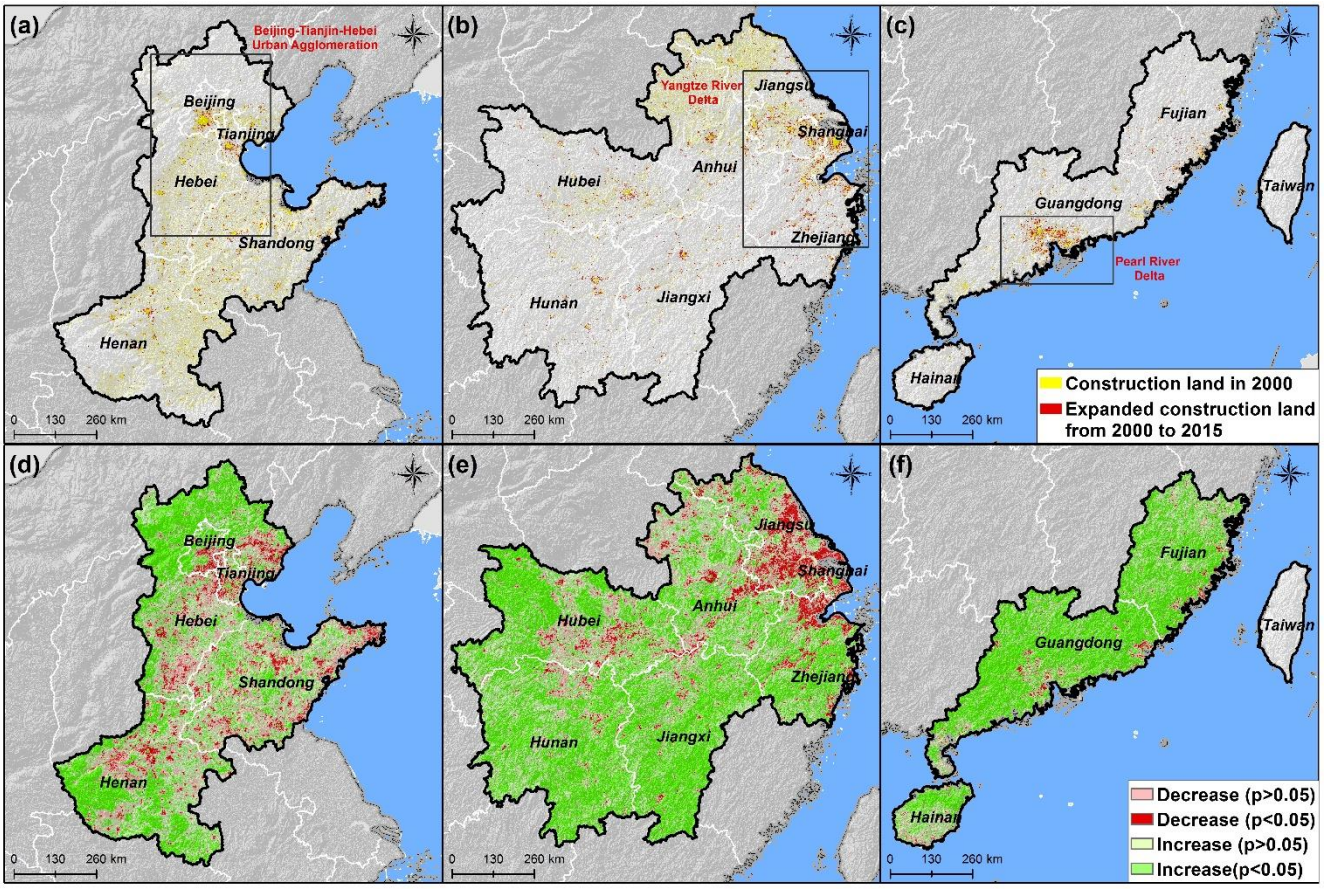

Figure 14. Change of construction land from 2000 to 2015: (a) HHHP; (b) MLYR; (c) SC; and the Change of EVI from 2000 to 2019:(d) HHHP; (e) MLYR; (f) SC.

Table 5. Changes in Forest Obtained from National Bureau of Statistics of China

Time period	Forest area (10^6 hm^2)	Accumulated afforested area (10^6 hm^2)	Forest coverage (%)
2004 ~ 2008	179.02	53.65	18.64
2009 ~ 2018	214.07	70.40	22.30
Change (2004 ~ 2018)	35.05 (19.6%)	3.14 (31.2%)	3.66 (19.6%)

Table 6. Changes in Croplands Obtained from National Bureau of Statistics of China

Time period	Harvested area (10^6 hm^2)	Total food production (10^6 t)	Effective irrigation area (10^6 hm^2)	Amount of fertilizer use (10^6 t)
2000 ~ 2008	154.31	476.95	55.19	46.48
2009 ~ 2018	163.31	620.99	64.14	57.94
Change (2000 ~ 2018)	9.00 (5.8%)	144.04 (30.2%)	8.96 (16.2%)	11.46 (24.7%)

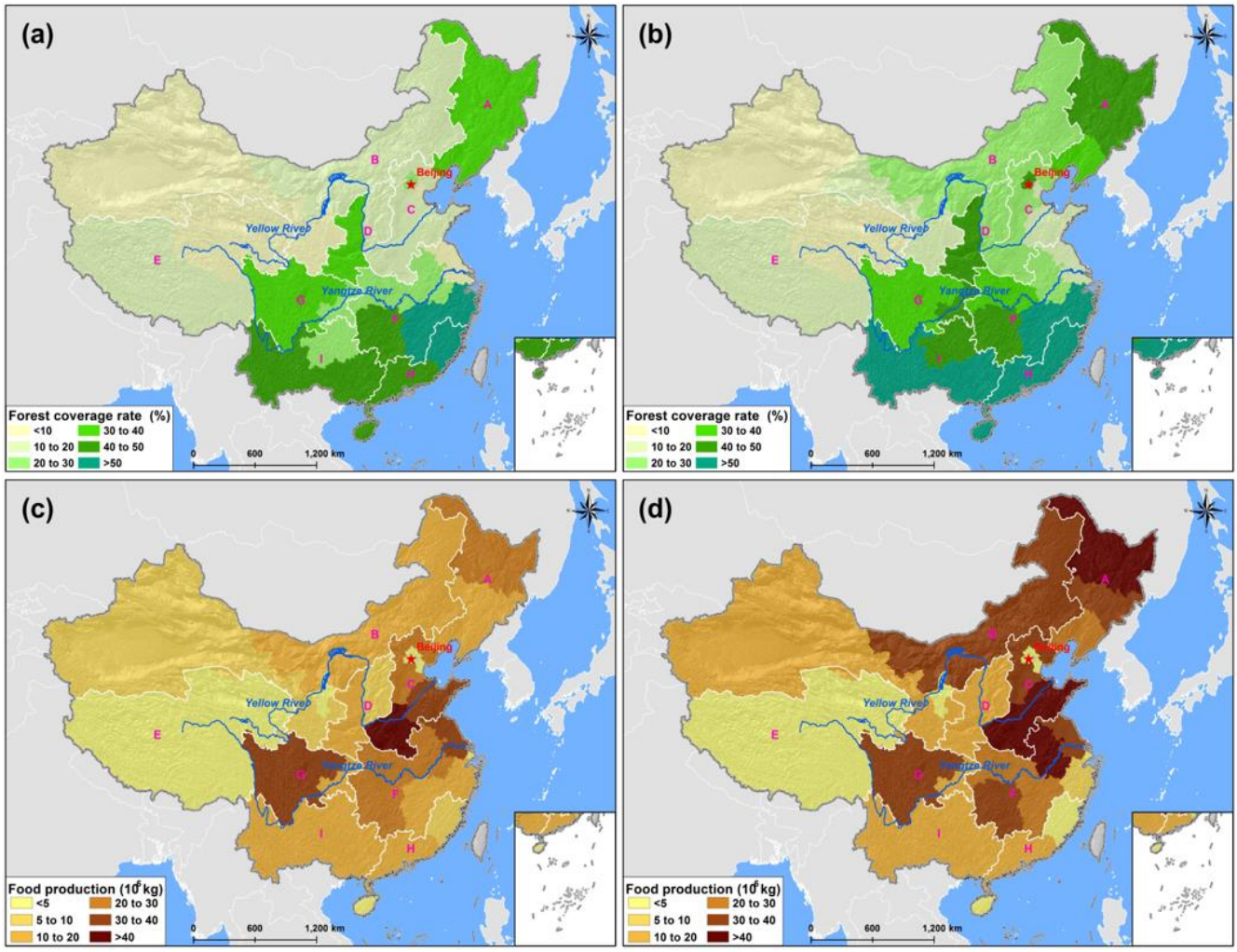

Figure 15. The forest coverage rate and total food production of different years. (a) forest coverage rate of 2004; (b) forest coverage rate of 2018; (c) total food production of 2000; (d) total food production of 2018.

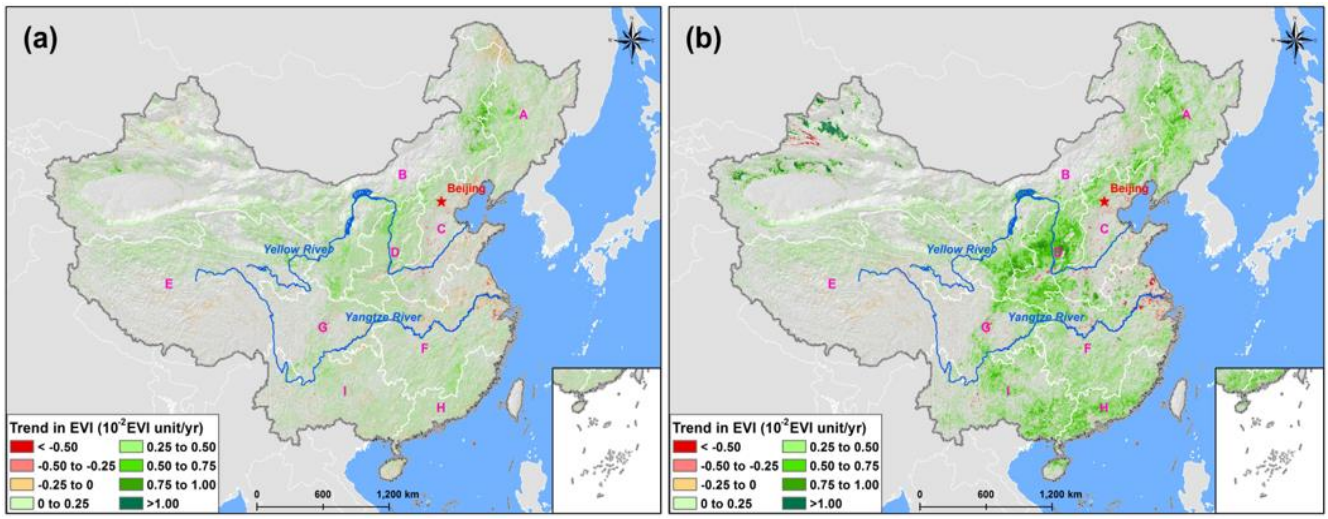

Figure 16. Trends of EVI_c (a) and EVI_h (b) in the regions where EVI show significant trends ($p < 0.05$) in mainland China during 2000 to 2019.

4.5.2. Relative Importance of Climate Change and Human Activities on EVI Variations

The EVI over mainland China was impacted by both climate change and human activities. The relative roles of climate change and human activities at the pixel level were showed in Figure 17. Combined impacts of climate change and human activities enhanced the EVI in 87.7% of the RST, whereas they reduced the EVI in only 3.8% of the area from 2000 to 2019. The decrease in EVI caused by the combined impacts of climate change and human activities were mainly distributed in Beijing-Tianjin-Hebei Urban Agglomeration and Yangtze River Delta. The change of EVI only driven by climate change or human activities was rarely found. Climate change was responsible for EVI increase in 1.6% of the RST and EVI decrease in 0.5% of the area. The increase in EVI dominated by climate change were mainly distributed in QTP and SBSR. Additionally, the human activities contributed to an increase in the EVI in 5.3% of the RST, which was greater than the percentage of the area (1.2%) showing a decrease. Considering the change in EVI, the contribution of climate change was about 0 to 40% in most areas of RST (accounted for 74.3%). Climate change was a dominant driver of EVI change ($Con_c \geq 60\%$) over only 9.9% of the areas of RST, mainly in Qinghai Province in QTP and Hexi Corridor in NASR. The human activities explained more than 60% of the observed significant trend in more than half areas of RST. They contributed the most ($Con_h \geq 80\%$) to the observed EVI trend over 28.0% of the RST, mainly in LP, NCP, southeastern YGP and northern SC (Figure 18).

5. Discussion

5.1. Comparison the Results with NDVI

Besides EVI, Normalized Difference Vegetation Index (NDVI) is also widely used for vegetation variations analysis. With the yearly NDVI data obtained from Resource and Environment Data Cloud Platform (RESDC) (http://www.resdc.cn/) and the same methods mentioned in Section 3, the spatial-temporal variation of NDVI can been analyzed. Proportions of vegetated lands showing greening/browning identified by EVI and NDVI were similar (Table 7). Temporal variations of vegetation from the two indexes agree (bule and red color in Figure 19) over 75.8% of the vegetated area and the disagreement (yellow and green color in Figure 19) is mostly in western and northern China where the vegetation is sparse. For example, In QTP and NASR, the temporal variations of vegetation from the two indexes disagree over 39.8 and 30.8% of the vegetated area respectively. The two greening clusters, namely NCR and LP, identified by NDVI were approximately matching in EVI data. And both NDVI trend and EVI trend showed that the browning vegetated area located in Beijing-Tianjin-Hebei Urban Agglomeration and Yangtze River Delta.

The spatiotemporal variation characteristics of NDVI in Yangtze River (YZRB) and Yellow River Basin (YRB), two extremely important basins in China, were studied by Zhang et al. (2020). The results suggest that the greening vegetated areas were mainly distributed in the central and eastern YRB and the central Yangtze River, while the east YZRB is browning. These

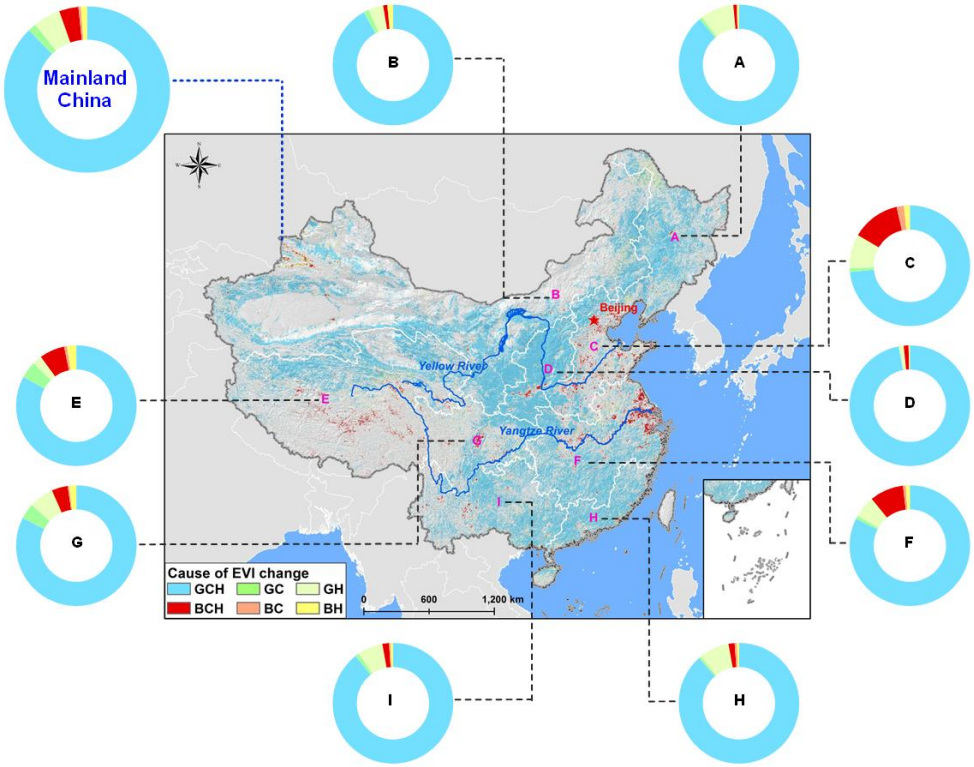

Figure 17. Spatial distribution of different driving forces of changes in EVI in the regions where EVI showed significant trends ($p < 0.05$) in mainland China during 2000 to 2019.

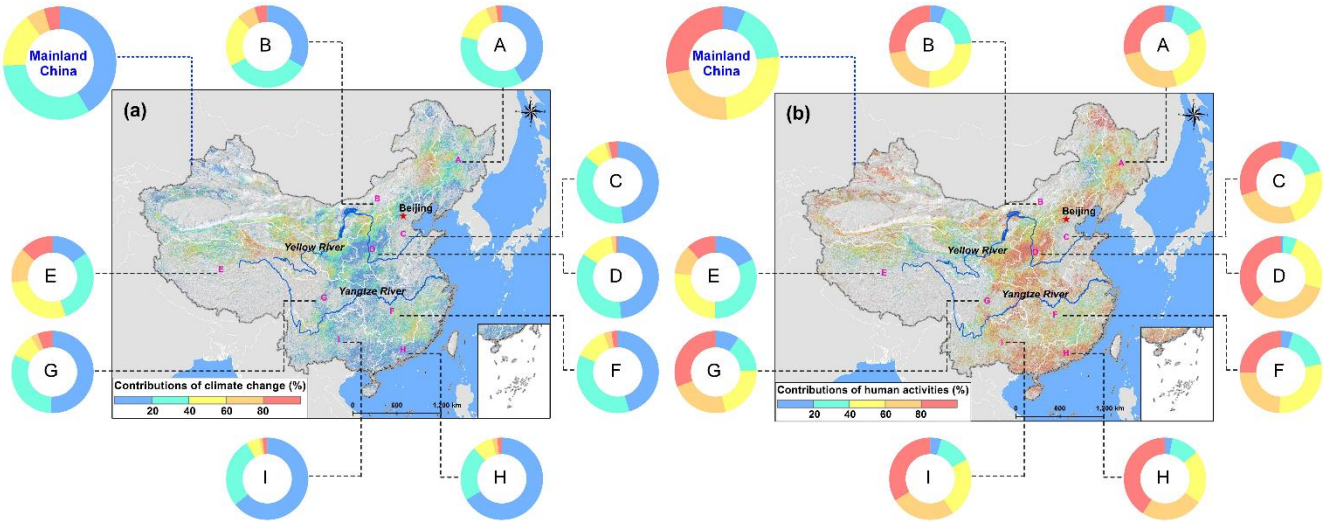

Figure 18. Contributions of climate change (a) and human activities (b) to EVI trend in the regions where EVI showed significant trends ($p < 0.05$) in China during 2000 to 2019.

Table 7. Changes in Vegetation Based on EVI and NDVI

Index and time period	Proportion of vegetated lands showing greening (%)	Proportion of vegetated lands showing browning (%)
NDVI (2000 to 2018)	80.1	19.9
EVI (2000 to 2019)	82.2	17.8

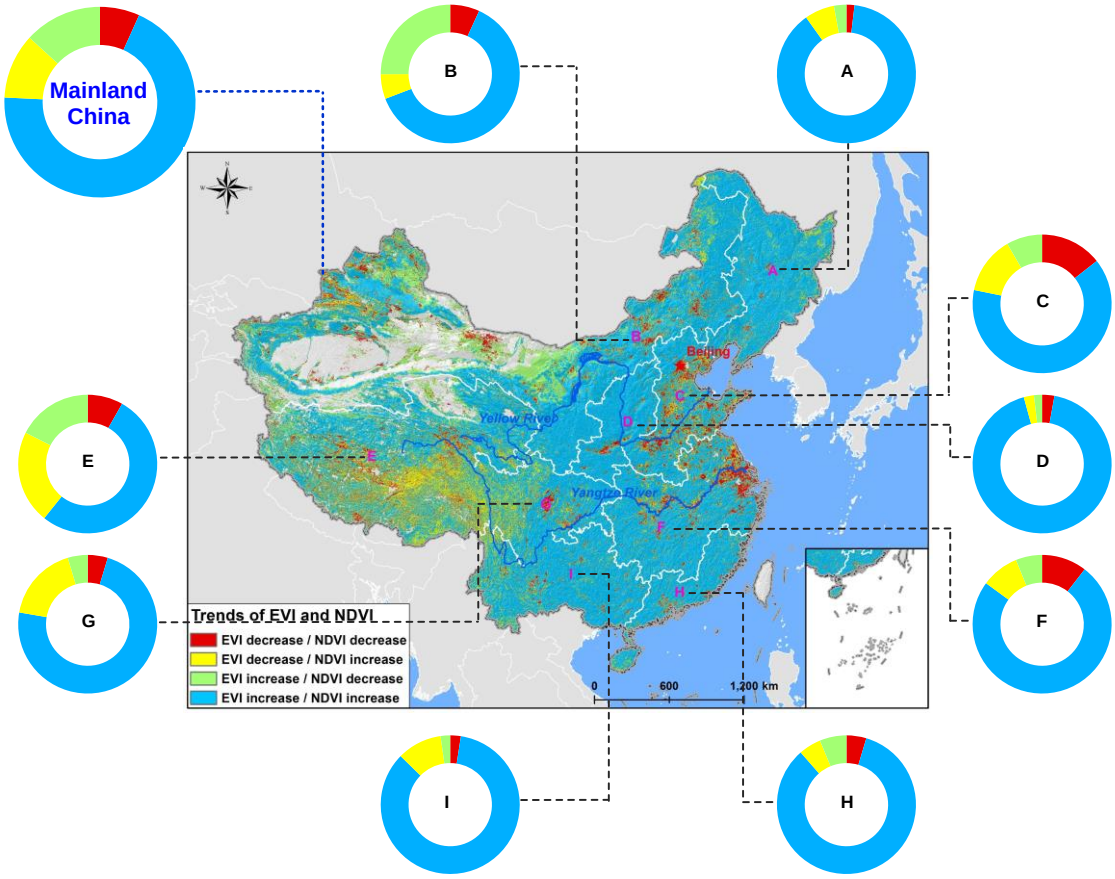

Figure 19. Comparison EVI trend and NVDI trend.

results are similar with our findings illustrated in Figure 7. Zhang et al. (2020) found that the climate change had greater influences on vegetation than that of human activities in the central area of the YZRB and YRB. In this study, we also detected that climate change was a dominant driver of EVI change in the middle reaches of Yellow River. However, the areas affected by climate change in YZRB mainly located in the upper reaches of Yangtze River, especially in Jinsha River Basin. It might be due to the different methods used for attribution analysis.

5.2. Impact of Climatic Factors on EVI

The precipitation and temperature were identified as leading climatic drivers determined the spatial-temporal of vegetation. Although their effects vary across climate zones, ecosystem types, biomes and plant species (Churkina and Running, 1998; Liu et al., 2015; Zhao et al., 2018). As shown in Figure 10, most of the mainland China (77.8%) experienced a warming and wetting trend during period 2000 to 2019. The areas with a warming and dryer climate accounted for 18.3% of the mainland China, mainly in HHHP (e.g., southern Haihe Plain), YGP (e.g., Hengduan Mountain region) and QTP (e.g., the south of Tanggula Mountain).

The dominant climate factors affecting EVI in different sub-regions was identified by correlation analysis (Table 2). The temperature was the most important climate factor contributing to vegetation growth in MLYR, SBSR and SC. These areas are rich in precipitation. In general, the water available for vegetation growth would not be limited by precipitation (Qu et al., 2020). It has been proven that the temperature plays an important role in controlling the green-up date in these regions. The study carried by Cong et al. (2012) showed that green-up date for broadleaf forest would advance by about one day with 1 °C of early growing season temperature increase. Maybe it is caused by the temperature increase in the beginning of the growing season, which may help to stimulate photosynthetic enzyme activities from the cold environment and ignite vegetation growth through its impacts on nutrient availability and uptake (Jarvis et al., 2000; Cristiano et al., 2014). An advancing trend in the beginning of vegetation growing season might lead to a prolonged length of vegetation growing season. Accordingly, the vegetation growth would be promoted. In contrast, precipitation made greater positive contribution for vegetation growth than temperature in NCP and especially, NASR. The average annual precipitation in NASR is 237.1 mm, the lowest level among the nine sub-basins and the vegetation growth is mostly restricted by precipitation. This finding is consistent with previous studies, which indicated that precipitation was the major limited factor for vegetation growth in this region (Hao et al., 2014; Yan et al., 2019). The response of EVI to climate factors in QTP was different from that in other regions. There were significant positive correlations of precipitation and temperature with EVI. Most of QTP are alpine and cold regions, with less precipitation and low temperature. It has been reported that the harsh climatic conditions are not favorite for vegetation growth, and thus both heat and water resources play crucial roles in maintaining and promoting vegetation status (Pan et al., 2017; Pang et al., 2017; Wang et al., 2017; Zheng et al., 2020). Because of wetter and warmer climatic conditions in recent decades in the whole QTP, the overall average EVI has increased. However, the vegetation degradation can still be found in local some areas, mainly because of the decrease of precipitation. Comparing with the temperature, the change of precipitation is more complicated. In the north of Tanggula Mountain (i.e., Qinghai), the effective precipitation increased in recent 20 years. However, a decrease trend was observed in the south of Tanggula Mountain (i.e., Tibet). The climate in most areas in Qinghai became warmer and wetter which contributes to the greening of alpine vegetation. But warmer and drier climate in most Tibet was the main factor for local vegetation degradation and this result accorded with the previous result presented by Li et al. (2016).

5.3. Impact of Human Activities on EVI

Human activities, especially afforestation projects, have been confirmed as the key factor to promotion of vegetation restoration (Qu et al., 2018; Chen et al., 2019). In order to combating desertification and land degradation, a series of programs for forests conservation and expansion have been carried out, which lead in greening of China. For example, the vegetation in LP has been greatly promoted owing to the Grain to Green Program (GGP), with over 21% of LP converting from low-value NDVI to high-value NDVI after the implementation of GGP (Li et al., 2017). The grassland productivity increased due to implementation of the GGP, especially in Shaanxi Province (5.89 $gC \cdot m^{-2} \cdot yr^{-1}$) (Yan et al., 2019). Based on ours analyses on accumulated afforested area change in mainland China, EVI was significantly correlated with the cumulative afforestation area, with $R = 0.852$ ($p < 0.01$), and areas where forest coverage rate increasing were consistent with the significant increase of EVI.

The study of Li et al. (2018) indicated that the vegetation degradation mainly be found in the more economically developed southern China and North China Plain, because of the transformation from cropland to urban land. The climate is becoming wetter and warmer in urban areas of these regions, which would promote vegetation growth. However, these positive effect on vegetation growth cannot offset the negative effect caused by rapid urbanization (Jiang et al., 2015). Beijing-Tianjin-Hebei Urban Agglomeration, Yangtze River Delta and Pearl River Delta are the important economic growth poles in China. Thus, a higher urbanization in the future is predictable. It might pose more pressure on ecosystem, such as vegetation degradation, if the local government does not implement any sustainable development. How to reconcile economic development with ecological protection is a considerable challenge. Establishment of more green spaces to increase vegetation cover in urbanized areas is an effective way to offset negative effects led by urbanization.

Inner Mongolia, located in NASR has witnessed the problem of grassland degeneration in recent decades. Grassland degeneration mainly located in Xilingol and Hulun Buir. Previous studies indicated that the grassland degeneration in Inner Mongolia caused by many factors, such as overgrazing, cultivated

land expansion (Zhou et al., 2014; Zhou et al., 2017). According to the Inner Mongolia Statistical Yearbook, the total number of livestock and the area of cultivated land increased by 48.2 and 26.7% respectively from 2000 to 2018. This increase can accelerate grassland degradation and resulting in further serious environmental problems (i.e., desertification, soil erosion, biodiversity decline). There is no doubt that the natural grassland plays an important role not only in animal production but also in carbon sequestration in Inner Mongolia or the whole NASR. It is necessary to find sustainable grassland management to support the increasing requirement for feed in the context of environment protection.

5.4. Limitations of the Study

Excepting the driving factors of vegetation dynamics considered in this study, atmospheric CO_2 concentration also has effect on greening, especially in the Northern Hemisphere (Zhu et al., 2016). Stomatal conductance and plant water use would be modified by higher CO_2 concentration, leading to a lower drought stress on vegetation growth, known as CO_2 fertilization (Swann et al., 2016). Besides, the complex interaction of climate change and human activities would affect vegetation variations. However, climate change and human activities were regarded as two independent driving forces, which might influence the accuracy of vegetation change attribution. Residual trend analysis method was used to quantify the impacts of climate change and human activities on vegetation variation, which was based on Multivariate Linear Regression. It exits some uncertainties associated with reconstruction of EVI_c series. Establishing a comprehensive model to separate the effects of climate change and human activities is needed in the future.

6. Conclusions

This study analyzed the vegetation changes and investigated the causal factors in the mainland China. The primary conclusions are as follows:

In general, the EVI is lower in the northwest and increases toward the southeast in mainland China. The EVI was normally lower than 0.30 in the Northwest China and higher than 0.50 in most southern China. A significantly increasing rate of EVI as the longitude increased can be observed, defining a green rate of 0.009 per degree in longitude.

The annual EVI for the entire mainland China showed a significant increase trend during 2000 to 2019, with a rate of 0.0023 per year. A break point in 2009 was detected and the increasing rate became weaker after 2009. The areas where the EVI having significant increase and decrease trends account for 42.1 and 2.7% of the vegetated land, respectively.

The wetter and warmer climatic condition in recent 20 years is conducive to vegetation growth in mainland China. The vegetation in northern China is more sensitive to precipitation while the temperature makes greater positive contribution to vegetation growth in southern China. However, in the Alpine region, both precipitation and temperature affected vegetation growth significantly. Anthropogenic factors, such as increase of forest planting and food production also played an important role in greening vegetation, especially in Loess Plateau, Northeast China Plain and Huang-Huai-Hai Plain. The browning in some vegetated land might relate to urbanization, such as Beijing-Tianjin-Hebei Urban Agglomeration, Yangtze River Delta and Pearl River Delta. Generally, human activities were the main driving factors of vegetation greening in mainland China in two decades. Implementation of ecological restoration programs, construction of irrigated areas and heavy fertilizer use promote the vegetation growth in forestland and cultivated land.

Acknowledgements. This research was funded by [National Key Research and Development Project] grant number [2017YFC1502404]; [National Natural Science Foundation of China] grant number [41890821, 52079008]; [National Public Research Institutes for Basic R&D Operating Expenses Special Project] grant number [CKSF2019212/SZ].

References

Adole, T., Dash, J. and Atkinson, P.M. (2018). Large-scale pre-rain vegetation green-up across Africa. *Glob. Change Biol.*, 24, 4054-4068. https://doi.org/10.1111/gcb.14310

Ahmed, T. and Singh, D. (2020). Probability Density Functions Based Classification of MODIS NDVI Time Series Data and Monitoring of Vegetation Growth Cycle. *Adv. Space Res.*, 66,873-886. https://doi.org/10.1016/j.asr.2020.05.004

Bégué, A., Vintrou, E., Ruelland, D., Claden, M. and Dessay, N. (2011). Can a 25-year trend in Soudano-Sahelian vegetation dynamics be interpreted in terms of land use change? A remote sensing approach. *Glob. Environ. Change*, 21(2), 413-420. https://doi.org/10.1016/j.gloenvcha.2011.02.002

Buyantuyev, A. and Wu, J. (2012). Urbanization diversifies land surface phenology in arid environments: Interactions among vegetation, climatic variation, and land use pattern in the Phoenix metropolitan region, USA. *Landsc. Urban Plan.*, 105(1-2), 149-159. https://doi.org/10.1016/j.landurbplan.2011.12.013

Chen, X., Zhang, X., Zhang, Y. and Wan, C. (2009). Carbon sequestration potential of the stands under the Grain for Green Program in Yunnan Province, China. *For. Ecol. Manag.*, 258(3), 199-206. https://doi.org/10.1016/j.foreco.2008.07.010

Churkina, G. and Running S.W. (1998). Contrasting climatic controls on the estimated productivity of global terrestrial biomes. *Ecosystems*, 1(2), 206-215. https://doi.org/10.1007/s100219900016

Cong, N., Piao, S., Chen, A., Wang, X., Lin, X., Chen, S., Han, S., Zhou, G. and Zhang, X. (2012). Spring vegetation green-up date in China inferred from SPOT NDVI data: A multiple model analysis. *Agric. For Meteorol.*, 165, 104-113. https://doi.org/10.1016/j.agrformet.2012.06.009

Cristiano, P., Madanes, N., Campanello, P., di Francescantonio, D., Rodríguez, S., Zhang, Y., Carrasco, L. and Goldstein, G. (2014). High NDVI and potential canopy photosynthesis of South American subtropical forests despite seasonal changes in leaf area index and air temperature. *Forests*. 5(2), 287-308. https://doi.org/10.3390/f5020287

Daham, A., Han D., Rico-Ramirez, M., and Marsh, A. (2018). Analysis of NVDI variability in response to precipitation and air temperature in different regions of Iraq, using MODIS vegetation indices. *Environ. Earth. Sci.*, 77, 389. https://doi.org/10.1007/s12665-018-7560-x

Deng, X., Huang, J., Rozelle, S., Zhang, J. and Li, Z. (2015). Impact of urbanization on cultivated land changes in China. *Land Use Policy*, 45, 1-7. https://doi.org/10.1016/j.landusepol.2015.01.007

Du, J., Fu, Q., Fang, S., Wu, J., He, P. and Quan, Z. (2019). Effects of rapid urbanization on vegetation cover in the metropolises of China over the last four decades. *Ecol. Indic.*, 107, 105458. https://doi.org/10.1016/j.ecolind.2019.105458

Fraga, H., Amraoui, M., Malheiro, A.C., Moutinho-Pereira, J., Eiras-Dias, J., Silvestre, J. and Santos, J.A. (2014). Examining the relationship between the enhanced vegetation index and grapevine phenology. *Eur. J. Remote. Sens.*, 47, 753-771. https://doi.org/10.5721/EuJRS20144743

Hao, L., Sun, G., Liu, Y., Gao, Z. and Wu, B. (2014). Effects of precipitation on grassland ecosystem restoration under grazing exclusion in Inner Mongolia, China. *Landsc. Ecol.*, 29(10), 1657-1673. https://doi.org/10.1007/s10980-014-0092-1

Herrmann, S.M., Anyamba, A. and Tucker, C.J. (2005). Recent trends in vegetation dynamics in the African Sahel and their relationship to climate. *Glob. Environ. Change*, 15, 394-404. https://doi.org/10.1016/j.gloenvcha.2005.08.004

Huete, A., Didan, K., Miura, T., Rodriguez, E.P., Gao, X. and Ferreira, L.G. (2002). Overview of the radiometric and biophysical performance of the MODIS vegetation indices. *Remote Sens. Env.*, 83(1-2), 195-213. https://doi.org/10.1016/S0034-4257(02)00096-2

Jarvis, P. and Linder, S., (2000). Constraints to growth of boreal forests. *Nature*, 405(6789), 904-905. https://doi.org/10.1038/35016154

Jiang, C., Wu, Z.F., Cheng, J., Yu, Q. and Rao, X.Q. (2015). Impacts of urbanization on net primary productivity in the Pearl River Delta, China. *Int. J. Plant Prod.*, 9(4), 581-598. https://doi.org/10.22069/IJPP.2015.2464

Kuenzer, C., Dech, S. and Wagner, W. (2015). Remote sensing time series revealing land surface dynamics: Status quo and the pathway ahead. *Remote Sensing Time Series. Remote Sensing and Digital Image Processing*. Springer, Cham., pp 1-24. https://doi.org/10.1007/978-3-319-15967-6_1

Kumar, P., Rani, M., Pandey, P.C., Majumdar, A. and Nathawat, M.S. (2010). Monitoring of deforestation and forest degradation using remote sensing and GIS: A case study of Ranchi in Jharkhand (India). *Rep. opinion*, 2(4), 14-20.

Li, J., Peng, S. and Li, Z. (2017). Detecting and attributing vegetation changes on China's loess plateau. *Agric. For Meteorol.*, 247, 260-270. https://doi.org/10.1016/j.agrformet.2017.08.005

Li, J., Wang, Z., Lai, C., Wu, X., Zeng, Z., Chen, X. and Lian, Y. (2018). Response of net primary production to land use and land cover change in mainland China since the late 1980s. *Sci. Total Environ.*, 639, 237-247. https://doi.org/10.1016/j.scitotenv.2018.05.155

Li, Q., Zhang, C., Shen, Y., Jia, W. and Li, J. (2016). Quantitative assessment of the relative roles of climate change and human activities in desertification processes on the Qinghai-Tibet Plateau based on net primary productivity. *Catena*, 147, 789-796. https://doi.org/10.1016/j.catena.2016.09.005

Liu, Y., Li, Y., Li, S. and Motesharrei, S. (2015). Spatial and temporal patterns of global NDVI trends: Correlations with climate and human factors. *Remote Sens.*, 7(10), 13233-13250. https://doi.org/10.3390/rs71013233

Muradyan, V., Tepanosyan, G., Asmaryan, S., Saghatelyan, A. and Dell'Acqua, F. (2019). Relationships between NDVI and climatic factors in mountain ecosystems: a case study of Armenia. *Remote Sensing Applications: Society and Environment*, 14, 158-169 https://doi.org/10.1016/j.rsase.2019.03.004.

Pan, T., Zou, X., Liu, Y., Wu, S. and He, G. (2017). Contributions of climatic and non-climatic drivers to grassland variations on the Tibetan Plateau. *Ecol. Eng.*, 108, 307-317. https://doi.org/10.1016/j.ecoleng.2017.07.039

Pang, G., Wang, X. and Yang, M. (2017). Using the NDVI to identify variations in, and responses of, vegetation to climate change on the Tibetan Plateau from 1982 to 2012. *Quat. Int.*, 444, 87-96. https://doi.org/10.1016/j.quaint.2016.08.038

Peng, W., Kuang, T. and Tao, S. (2019). Quantifying influences of natural factors on vegetation NDVI changes based on geographical detector in Sichuan, western China. *J. Clean. Prod.*, 233,353-367. https:// doi.org/10.1016/j.jclepro.2019.05.355

Piao, S., Fang, J., Ciais, P., Peylin, P., Huang, Y., Sitch, S. and Wang, T. (2009). The carbon balance of terrestrial ecosystems in China. *Nature*, 458(7241), 1009-1013. https://doi.org/10.1038/nature07944

Piao, S.L., Nan, H.J., Huntingford, C., Ciais, P., Friedlingstein, P., Sitch, S., Peng, S.S., Ahlstrom, A., Canadell, J.G., Cong, N., Levis, S., Levy, P.E., Liu, L.L., Lomas, M.R., Mao, J.F., Myneni, R.B., Peylin, P., Poulter, B., Shi, X.Y., Yin, G.D., Viovy, N.,Wang, T.,Wang, X.H., Zaehle, S., Zeng, N., Zeng, Z.Z. and Chen, A.P. (2014). Evidence for a weakening relationship between interannual temperature variability and northern vegetation activity. *Nat. Commun.*, 5(1), 1-7. https://doi.org/10.1038/ncomms6018

Qu, S., Wang, L., Lin, A., Yu, D. and Li, C. (2020). Distinguishing the impacts of climate change and anthropogenic factors on vegetation dynamics in the Yangtze River Basin, China. *Ecol. Indic.*, 108, 105724. https://doi.org/10.1016/j.ecolind.2019.105724

Qu, S., Wang, L., Lin, A., Zhu, H. and Yuan, M. (2018). What drives the vegetation restoration in Yangtze River basin, China: Climate change or anthropogenic factors? *Ecol. Indic.*, 90, 438-450. https://doi.org/10.1016/j.ecolind.2018.03.029

Raynolds, M.K., Comiso, J.C., Walker, D.A. and Verbyla, D. (2008). Relationship between satellite-derived land surface temperatures, arctic vegetation types, and NDVI. *Remote Sens. Environ.*, 112(4), 1884-1894. https://doi.org/10.1016/j.rse.2007.09.008

Setiawan, Y., Yoshino, K. and Prasetyo, L.B. (2014). Characterizing the dynamics change of vegetation cover on tropical forestlands using 250 m multi-temporal MODIS EVI. *Int. J. Appl. Earth Obs. Geoinf.*, 2014,26,132-144. https://doi.org/10.1016/j.jag.2013.06.008

Shi, Y., Jin, N., Ma, X., Wu, B., He, Q., Yue, C. and Yu, Q. (2020). Attribution of climate and human activities to vegetation change in China using machine learning techniques. *Agric. For. Meteorol.*, 294, 108146. https://doi.org/10.1016/j.agrformet.2020.108146

Sitch, S., Huntingford, C., Gedney, N., Levy, P., Lomas, M., Piao, S., Betts, R., Ciais, P., Cox, P., Friedlingstein, P., Jones, C.D, Prentice, I.C and Woodward, F.I (2008). Evaluation of the terrestrial carbon cycle, future plant geography and climate-carbon cycle feedbacks using five Dynamic Global Vegetation Models (DGVMs). *Glob. Change Biol.*, 14(9), 2015-2039. https://doi.org/10.1111/j.1365-2486.2008.01626.x

Swann, A.L.S., Hoffman, F.M., Koven, C.D. and Randerson, J.T. (2016). Plant responses to increasing CO_2 reduce estimates of climate impacts on drought severity. *PNAS*, 113(36), 10019. https://doi.org/10.1073/pnas.1604581113

Szabo, S., László, E., Kovács, Z., Püspöki, Z., Kertesz, A., Singh, S., and Bertalan-Balazs, B. (2018). NDVI dynamics as reflected in climatic variables: spatial and temporal trends-a case study of Hungary. *GISci. & Remote Sensing*, 57. 1-26. 10.1080/15481603.2018.1560686.

Tian, Z., Zhang, D. and He, X. (2019). Spatio-temporal variations in vegetation net primary productivity and their driving factors in Yellow River Basin from 2000 to 2015. *Res. Soil Water Conserv.*, 26(2), 255-262.

Vijith, H. and Dodge-Wan, D. (2020). Applicability of MODIS land cover and Enhanced Vegetation Index (EVI) for the assessment of spatial and temporal changes in strength of vegetation in tropical rainforest region of Borneo. *Remote Sens. App: Soc. Env.*, 18, 100311. https://doi.org/10.1016/j.rsase.2020.100311

Wang, Z., Xie, P., Lai, C., Chen, X., Wu, X., Zeng, Z. and Li, J. (2017). Spatiotemporal variability of reference evapotranspiration and contributing climatic factors in China during 1961-2013. *J. Hydrol.*, 544, 97-108. https://doi.org/10.1016/j.jhydrol.2016.11.021

Wang, Z., Zhang, Y., Yang, Y., Zhou, W., Gang, C., Zhang, Y., Li, J.,

An, R., Wang, K., Odeh, I. and Qi, J. (2016). Quantitative assess the driving forces on the grassland degradation in the Qinghai-Tibet Plateau, in China. *Ecol. Inform.*, 33, 32-44. https://doi.org/10.1016/j.ecoinf.2016.03.006

Wang, Z., Zhao, T., Hou, M. and Yan, X. (2013). Vegetation index trends for the northern part of China at the beginning of the 21st century. *Clim. Envi. Res.*, 18(2), 156-164 (in Chinese).

Wessels, K.J., Prince, S.D., Malherbe, J., Small, J., Frost, P.E. and VanZyl, D. (2007). Can human-induced land degradation be distinguished from the effects of rainfall variability? A case study in South Africa. *J. Arid Environ.*, 68, 271-297. https://doi.org/10.1016/j.jaridenv.2006.05.015

Xu, L., Myneni, R.B., Chapin III, F.S, Callaghan, T.V., Pinzon, J.E., Tucker, C.J., Zhu, Z., Bi, J., Ciais, P., Tømmervik, H., Euskirchen, E.S., Forbes, B.C., Piao, S.L., Anderson, B.T., Ganguly, S., Nemani, R.R., Goetz, S.J., Beck, P.S.A., Bunn, A.G., Cao, C. and Stroeve, J.C. (2013). Temperature and vegetation seasonality diminishment over northern lands. *Nat. Clim. Change*, 3(6), 581-586. https://doi.org/10.1038/nclimate1836

Xu, X., Lin, H., Hou, L. and Yao, X. (2002). An assessment for sustainable developing capability of integrated agricultural regionalization in China. *Chi. Geol. Sci.*, 12(1), 1-8. https://doi.org/ 10.1007/s11769-002-0063-3

Yan, Y., Liu, X., Wen, Y. and Ou, J. (2019). Quantitative analysis of the contributions of climatic and human factors to grassland productivity in northern China. *Ecol. Indic.*, 103, 542-553. https://doi.org/10.1016/j.ecolind.2019.04.020

Yang, M., Mou, Y., Meng, Y., Liu, S., Peng, C. and Zhou, X. (2020). Modeling the effects of precipitation and temperature patterns on agricultural drought in China from 1949 to 2015. *Sci. Total. Environ.*, 711, 135139. https://doi.org/10.1016/j.scitotenv.2019.135139

Yin, L., Dai, E., Zheng, D., Wang, Y. Ma, L. and Tong, M. (2020). What drives the vegetation dynamics in the Hengduan Mountain region, Southwest China: Climate change or human activity?. *Ecol. Indic.*, 112, 106013. https://doi.org/10.1016/j.ecolind.2019.106013

Yuan, Z., Xu, J., Chen, J., Huo, J., Yu, Y., Locher, P. and Xu, B. (2017). Drought assessment and projection under climate change: A case study in the middle and lower Jinsha River Basin. *Adv. Meteorol.*, ID5757238. https://doi.org/10.1155/2017/5757238

Yuan, Z., Yan, D., Yang, Z., Yin, J and Yuan, Y. (2015). Temporal and spatial variability of drought in Huang-Huai-Hai River Basin, China. *Theor. Appl. Climatol.*, 122(3-4), 755-769. https://doi.org/10.1007/s00704-014-1332-7

Yuan, Z., Yan, D., Yang, Z., Yin, J., Zhang, C. and Yuan, Y. (2017). Projection of surface water resources in the context of climate change in typical regions of China. *Hydrol. Sci. J.*, 62(2), 283-293. https://doi.org/10.1080/02626667.2016.1222531

Zhang, P., Cai, Y., Yang, W., Yi, Y., Yang, Z. and Fu, Q. (2019). Multiple spatio-temporal patterns of vegetation coverage and its relationship with climatic factors in a large dam-reservoir-river system. *Ecol. Eng.*, 138, 188-199. https://doi.org/10.1016/j.ecoleng.2019.07.016

Zhang, W., Wang, L., Xiang, F., Qin, W. and Jiang, W. (2020). Vegetation dynamics and the relations with climate change at multiple time scales in the Yangtze River and Yellow River Basin, China. *Ecol. Indic.*, 110, 105892. https://doi.org/10.1016/j.ecolind.2019.105892

Zhang, Y., Peng, C., Li, W., Tian, L., Zhu, Q., Chen, H., Fang, X., Zhang, G., Liu, G., Mu, X., Li, Z., Li, S., Yang, Y., Wang, J. and Xiao, X. (2016). Multiple afforestation programs accelerate the greenness in the 'three North' region of China from 1982 to 2013. *Ecol. Indic.*, 61, 404-412. https://doi.org/10.1016/j.ecolind.2015.09.041

Zhao, L., Dai, A. and Dong, B. (2018). Changes in global vegetation activity and its driving factors during 1982-2013. *Agric. For. Meteorol.*, 249, 198-209. https://doi.org/10.1016/j.agrformet.2017.11.013

Zhao, M. and Running, S.W. (2010). Drought-induced reduction in global terrestrial net primary production from 2000 through 2009. *Science*, 329(5994), 940-943. https://doi.org/10.1126/science.1192666

Zheng, K., Wei, J., Pei, J., Cheng, H., Zhang, X., Huang, F., Li, F. and Ye, J. (2019). Impacts of climate change and human activities on grassland vegetation variation in the Chinese Loess Plateau. *Sci. Total Environ.*, 660, 236-244. https://doi.org/10.1016/j.scitotenv.2019.01.022

Zheng, Z., Zhu, W. and Zhang, Y. (2020). Seasonally and spatially varied controls of climatic factors on net primary productivity in alpine grasslands on the Tibetan Plateau. *Glob. Ecol. Conserv.*, 21, e00814. https://doi.org/10.1016/j.gecco.2019.e00814

Zhou, W., Gang, C., Zhou, L., Chen, Y., Li, J., Ju, W. and Odeh, I. (2014). Dynamic of grassland vegetation degradation and its quantitative assessment in the northwest China. *Acta Oecol.*, 55, 86-96. https://doi.org/10.1016/j.actao.2013.12.006

Zhou, W., Yang, H., Huang, L., Chen, C., Lin, X., Hu, Z. and Li, J. (2017). Grassland degradation remote sensing monitoring and driving factors quantitative assessment in China from 1982 to 2010. *Ecol. Indic.*, 83, 303-313. https://doi.org/10.1016/j.ecolind.2017.08.019

Zhou, Y., Zhang, L., Fensholt, R., Wang, K., Vitkovskaya, I. and Tian, F. (2015). Climate contributions to vegetation variations in central Asian drylands: Pre-and post-USSR collapse. *Remote Sens.*, 7(3), 2449-2470. https://doi.org/10.3390/rs70302449

Zhu, Z., Piao, S., Myneni, R.B., Huang, M., Zeng, Z., Canadell, J.G., Ciais, P., Sitch, S., Friedlingstein, P., Arneth, A., Cao, C., Cheng, L., Kato, E., Koven, C., Li, Y., Lian, X., Liu, Y., Liu, R., Mao, J., Pan, Y., Peng, S., Peñuelas, J., Poulter, B., Pugh, T.A.M., Stocker, B.D., Viovy, N., Wang, X., Wang, Y., Xiao, Z., Yang, H., Zaehle, S. and Zeng, N. (2016). Greening of the Earth and its drivers. *Nat. Clim. Change*, 6(8), 791-795. https://doi.org/10.1038/nclimate3004